arXiv:1405.2849v3 [cond-mat.soft] 8 Oct 2015

Phase diagram of mixtures of colloids and polymers in the thermal crossover from good to θ solvent.

Giuseppe D'Adamo*
SISSA, V. Bonomea 265, I-34136 Trieste, Italy

Andrea Pelissetto†
Dipartimento di Fisica, Sapienza Università di Roma and INFN, Sezione di Roma I, P.le Aldo Moro 2, I-00185 Roma, Italy

Carlo Pierleoni‡
Dipartimento di Scienze Fisiche e Chimiche, Università dell'Aquila and CNISM, UdR dell'Aquila, V. Vetoio 10, Loc. Coppito, I-67100 L'Aquila, Italy

(Dated: October 9, 2015)

We determine the phase diagram of mixtures of spherical colloids and neutral nonadsorbing polymers in the thermal crossover region between the θ point and the good-solvent regime. We use the generalized free-volume theory (GFVT), which turns out to be quite accurate as long as $q = R_g/R_c \lesssim 1$ (R_g is the radius of gyration of the polymer and R_c is the colloid radius). Close to the θ point the phase diagram is not very sensitive to solvent quality, while, close to the good-solvent region, changes of the solvent quality modify significantly the position of the critical point and of the binodals. We also analyze the phase behavior of aqueous solutions of charged colloids and polymers, using the extension of GFVT proposed by Fortini *et al.*, J. Chem. Phys. **128**, 024904 (2008).

PACS numbers: 61.25.he, 65.20.De, 82.35.Lr

I. INTRODUCTION

Mixtures of colloids and polymers are physical systems of great interest for their many technological applications. In particular, they are used, e.g., in the production of inks, paints, and personal-care products. There is also an extensive theoretical interest, since the addition of polymers to a colloid suspension can induce aggregation and allows one to modify the rheological properties in a controlled fashion. Here, we will consider dispersions of spherical colloids and nonadsorbing neutral polymers in an organic solvent. These systems show[1–6] a very interesting phenomenology, which only depends to a large extent on the nature of the solvent and on the ratio $q \equiv R_g/R_c$, where R_g is the zero-density radius of gyration of the polymer and R_c is the radius of the colloid. Experiments and numerical simulations indicate that such polymer-colloid mixtures have a solid colloidal phase for large enough colloidal concentrations and a corresponding fluid-solid coexistence. The presence of a fluid-fluid coexistence of a colloid-rich, polymer-poor phase (colloid liquid) with a colloid-poor, polymer-rich phase (colloid gas) is much less obvious. Extensive theoretical and experimental work indicates that such a transition occurs only if the size of the polymers is sufficiently large, i.e., for $q > q_{CEP}$, where[1] $q_{CEP} \approx 0.3$-0.4.

The phase behavior of colloid-polymer mixtures depends on solvent quality. If the polymer solution is close to the θ point, polymers behave approximately as ideal chains—the second virial coefficient is approximately equal to zero. In this regime, the Asakura-Oosawa-Vrij (AOV) model,[7,8] which gives a coarse-grained description of the mixture, provides quantitatively accurate results as long as $q \lesssim 1$. The polymers are treated as an ideal gas of point particles, which interact with the colloids by means of a simple hard-core potential. This model is extremely crude since it ignores the polymeric structure. Nonetheless, it correctly predicts polymer-colloid demixing as a result of the entropy-driven effective attraction (depletion interaction) between colloidal pairs due to the presence of the polymers.[9–21] Polymer-polymer interactions, which are necessary for a correct description of the good-solvent regime, have also been included. Refs. 22–25 discuss phenomenological generalizations of the AOV model, while Refs. 14,26–29 discuss coarse-grained models in which the polymer-colloid and polymer-polymer potentials are derived either numerically[14,26] from full-monomer simulations or by means of general theoretical considerations.[27–29] Another successfull approach is free-volume theory[10] which has been originally developed for mixtures of colloids and ideal polymers and later generalized to include polymer-polymer and polymer-colloid interactions.[5,30–33] Also the PRISM approach,[34–36] density functional theory,[22,37] and thermodynamic perturbation theory[38,39] have been used. Full-monomer simulations have also been performed,[40–43] providing the phase diagram in the protein regime $q \gtrsim 1$, in which coarse-grained models, which identify each polymer with a monoatomic molecule, are not expected to be accurate. For a comparison with experimental data, polydispersity effects should also be included as they affect quite significantly the thermodynamics of polymer solutions.[44,45] They are discussed in Refs. 46,47, where it is shown that gas-liquid phase separation is favored and fluid-solid segregation is retarded by increased polydispersity at fixed distribution of the polymer sizes.

While significant work has been devoted to polymer systems under good-solvent conditions or at the θ point, no systematic investigation has been performed of colloid-polymer segregation in the thermal crossover region. Such a regime can be parametrized by using the Zimm-Stockmayer-Fixmann variable[48]

$$z = a^{(1)} \frac{(T - T_\theta)}{T_\theta} M_w^{1/2}, \tag{1}$$

where T is the temperature (in K), T_θ its value at the θ point, M_w is the weight average molar mass[49] (equivalently, one could use the degree of polymerization L), and $a^{(1)}$ is a constant which is fixed once the normalization of z is specified. The θ point corresponds to $z = 0$, while the good-solvent regime corresponds to $z = \infty$. Choice (1) is not unique. Another slightly different parametrization which is often used in the experimental analyses is

$$z = a^{(2)} \frac{(T - T_\theta)}{T} M_w^{1/2}, \tag{2}$$

which differs by the presence of T, instead of T_θ, in the denominator. A third possibility, which is the one preferred by theorists, is

$$z = a^{(3)} (T - T_\theta) L^{1/2}, \tag{3}$$

where L is the degree of polymerization, i.e. the number of monomers present in each chain.

Note that Eqs. (1), (2), and (3) are approximations that neglect[44] logarithmic corrections in $\ln M_w$ or $\ln L$ and that, moreover, are only valid close to θ point. Indeed, in general[44] z is related to the temperature T by $z = \alpha_1 f_T(T) L^{1/2} (\ln L)^{-4/11}$ (or with M_w replacing L), where $f_T(T)$ is an analytic function vanishing at the θ point and α_1 is a system-dependent constant. However, as we show in the supplementary material[50] for three typical polymer solutions, the previous simple parametrizations without the logarithmic factor are fully adequate to describe experimental data in a large temperature interval, given the typical experimental accuracy.

In this work we aim at determining the phase behavior of colloid-polymer mixtures in the intermediate crossover region in which z is finite and positive. We will use the generalized free-volume theory[5,30–33] (GFVT), which has been shown to be quite accurate both at the θ point and under good-solvent conditions. To implement the GFVT approach, one needs explicit expressions for the polymer equation of state and for the depletion thickness[33] as a function of the polymer density and of z. We will use here the accurate results reported in Refs. 51–53. The GFVT results will be compared with numerical full-monomer data (a meaningful comparison requires an extrapolation of the numerical results to the scaling, $L \to \infty$, limit) and experimental results. It turns out that GFVT is only predictive for $q \lesssim 1$. For larger values of q, significant discrepancies are observed. This is not surprising given that GFVT treats polymers as soft colloids, an approximation that only makes sense for q small. Finally, we will consider the generalized model of Fortini *et al.*,[54] which allows one to determine the main features of the phase diagram of aqueous solutions of charged colloids.

The paper is organized as follows. In Section II we introduce the general ideas that allow us to describe the thermal crossover in terms of the two-parameter model variable z (a more extensive discussion can be found in Ref. 51). In Section III we define GFVT and validate its use against full-monomer results in the homogeneous phase for two values of q, $q = 1$ and $q = 2$. In Section IV we determine the phase diagram of the system as a function of q and z and carefully compare the results with previous work. In Section V we extend the discussion to dispersions of charged colloids. Finally, in Section VI we present our conclusions. In the supplementary material[50] we collect the relevant formulae for the polymer equation of state and the polymer-colloid depletion thickness that are used throughout the paper, and provide extensive tables of results. Moreover, we reanalize the experimental data presented in Refs. 55–58 and discuss carefully the effects of polydispersity. In particular, we determine the nonuniversal constants that allow us to map the experimental data onto the two-parameter model expressions we use to parametrize thermodynamic experimental quantities in the thermal crossover region.

II. THERMAL CROSSOVER FOR POLYMER SOLUTIONS

In this paper we consider polymer solutions in the thermal crossover regime, which is observed in a relatively large temperature interval above the θ temperature T_θ.[59] For $T \gg T_\theta$ in which interactions are dominated by the pairwise repulsion (good-solvent regime), polymers are swollen and the radius of gyration R_g scales as[60,61] L^ν, where[62] $\nu = 0.587597(7) \simeq 3/5$ is the Flory exponent. On the other hand, for $T = T_\theta$, polymers behave approximately as noninteracting random chains and $R_g \sim L^{1/2}$. In the intermediate region experiments and computer simulations show that, for sufficiently large values of the degree of polymerization L (i.e., for large molar masses M_w), thermodynamic and large-scale structural properties of the solution obey general relations of the form

$$\mathcal{O}(T, L, \rho_p) = \alpha_2 \mathcal{O}_G(L, \rho_p) f_{\mathcal{O}}(z, \phi_p), \tag{4}$$

where $\mathcal{O}_G(L, \rho_p)$ is the expression of $\mathcal{O}$ for the Gaussian-chain model, the function $f_{\mathcal{O}}$ is a universal—hence independent of chemical details—*crossover* function, $\rho_p = N_p/V$ is the number concentration of the polymers, $\phi_p = 4\pi R_g^3 \rho_p/3$, R_g is the *zero-density* radius of gyration, and α_2 is a nonuniversal constant that embodies all chemical details. The quantity z is the Zimm-Stockmayer-Fixmann variable defined in Eqs. (1), (2), or (3). By varying z one obtains the full crossover behavior, from the θ region, corresponding to small values of z, to the

good-solvent regime, which is obtained for $z \to \infty$.

Theory[44,63,64] supports the scaling behavior (4), albeit with a slightly different scaling variable. Indeed, the crossover limit should be taken by keeping $\alpha_1(T - T_\theta)L^{1/2}(\ln L)^{-4/11}$ fixed, which differs by a power of $\ln L$ from the scaling variable $z \sim (T - T_\theta)L^{1/2}$. Such a logarithmic dependence is irrelevant in most practical applications, since the observation of this slowly varying term would require accurate data in a very large interval of polymer lengths/molecular weights, both in experiments and in numerical simulations. Moreover, additive logarithmic corrections, vanishing as inverse powers of $1/\ln L$, should also be considered. They are expected to be relevant only very close to the θ point. For instance, they are responsible for the nonideal density corrections to the (osmotic) pressure P at T_θ. Indeed, if the θ point is defined as the temperature at which the second virial coefficient vanishes for each value of L, then we have $P = k_B T \rho_p (1 + a\rho_p^2)$, with[44,63,65] $a \propto 1/\ln L$. In this work, we do not consider such terms, assuming that L is so large that such corrections are negligible.

It is important to note that the nontrivial universal behavior is obtained by taking simultaneously the limits $L \to \infty$, $T \to T_\theta$, and $\rho_p \to 0$ (dilute and semidilute regime) in such a way that the arguments z and ϕ_p of the crossover function $f_{\mathcal{O}}$ remain constant. If the limits are taken differently, one would obtain a different result. For instance, in the zero-density case, if one takes the limit $L \to \infty$ at fixed $T > T_\theta$, one would obtain good-solvent behavior in all cases, while, if one decreases T towards T_θ at fixed large L, only the θ behavior would be observed. Analogously, if one takes the limit $L \to \infty$ at fixed ρ_p, one ends up with a melt.

Experimentally, the quality of the solution is usually determined by measuring the swelling ratio α in the zero-concentration limit or the second virial combination $A_{2,pp}$ (in the experimental literature, one often quotes the interpenetration ratio $\Psi = 2(4\pi)^{-3/2} A_{2,pp}$). The first quantity,

$$\alpha(T, L) = \frac{R_g(T, L)}{R_g(T_\theta, L)} \tag{5}$$

measures how the radius of gyration in the zero-concentration limit changes as T is increased away from T_θ. It varies from 1 to a number of order $L^{\nu-1/2}$ (it tends to infinity in the scaling limit $L \to \infty$) as T increases. The combination $A_{2,pp}$ is defined as

$$A_{2,pp}(T, L) = \frac{B_{2,pp}(T, L)}{R_g(T, L)^3}, \tag{6}$$

where $B_{2,pp}(T, L)$ is the second virial coefficient[66] defined by the expansion of the (osmotic) pressure P of the pure polymer solution,

$$P = k_B T \rho_p (1 + B_{2,pp}\rho_p + \ldots). \tag{7}$$

For $L \to \infty$, both functions $\alpha(T, L)$ and $A_{2,pp}(T, L)$ converge to functions $\alpha(z)$ and $A_{2,pp}(z)$, which are universal provided one chooses appropriately the constant $a^{(1)}$ appearing in Eq. (1). If the other definitions are used, $a^{(2)}$ or $a^{(3)}$ should be chosen appropriately. We will fix these constants by requiring that $A_{2,pp}(z) \approx 4\pi^{3/2} z$, or equivalently $\Psi \approx z$, for $z \to 0$. For large z, $A_{2,pp}$ converges to the good-solvent value,[67] $A_{2,pp}(z) = 5.50 + O(z^{-\Delta})$, where[62] $\Delta = 0.528(12)$, while $\alpha(z) \sim z^{2\nu-1}$. Because of universality, the z dependence of these two quantities can be determined in any model which describes the thermal crossover. High-precision numerical simulations of lattice polymer models provided an accurate expression for these two functions:[68]

$$A_{2,pp}(z) = 4\pi^{3/2} z (1 + 19.1187 z + 126.783 z^2 + 331.99 z^3 + 268.96 z^4)^{-1/4}, \tag{8}$$

and

$$\alpha(z) = (1 + 10.9288 z + 35.1869 z^2 + 30.4463 z^3)^{0.0583867}. \tag{9}$$

To determine the z dependence of the phase diagram, we have considered in detail the behavior for two values of z: $z = z^{(1)} = 0.056215$ and $z = z^{(3)} = 0.321650$, which correspond to[68] $A_{2,pp}(z^{(1)}) = 0.9926(10)$ and $A_{2,pp}(z^{(3)}) = 2.9621(27)$. Since $A_{2,pp} \approx 5.50$ under good-solvent conditions,[67] we have $A_{2,pp}(z)/A_{2,pp}(z = \infty) = 0.18$ and 0.54 for $z = z^{(1)}$ and $z = z^{(3)}$, respectively. Hence, the solution is quite close to the θ point for $z = z^{(1)}$, while for $z = z^{(3)}$ the behavior is intermediate between the good-solvent and the θ regimes. In Fig. 1 we report the lines $z = z^{(1)}$ and $z = z^{(3)}$ in the $(\Delta T, M_w)$ plane for three experimental systems, which are analyzed in detail in the supplementary material.[50] For the typical molar masses used in experiments, systems with $z = z^{(1)}$ correspond to temperatures that are only a few degrees above T_θ. Significantly larger temperature differences occur instead for $z = z^{(3)}$. In this case the solution is quite far from θ conditions.

III. GENERALIZED FREE-VOLUME THEORY

A. Definitions

We work in the semigrand canonical ensemble, in which the fundamental thermodynamic variables are the volume V, the temperature T, the number of colloids N_c, and the polymer chemical potential μ_p. In practice, it is more convenient to use as basic variables the crossover variable z (it will be always implicit in the notation), the colloid volume fraction ϕ_c defined by

$$\phi_c = V_c \frac{N_c}{V}, \tag{10}$$

where $V_c = 4\pi R_c^3/3$ is the volume of the colloid, and the reservoir polymer volume fraction $\phi_p^{(r)}$, which is re-

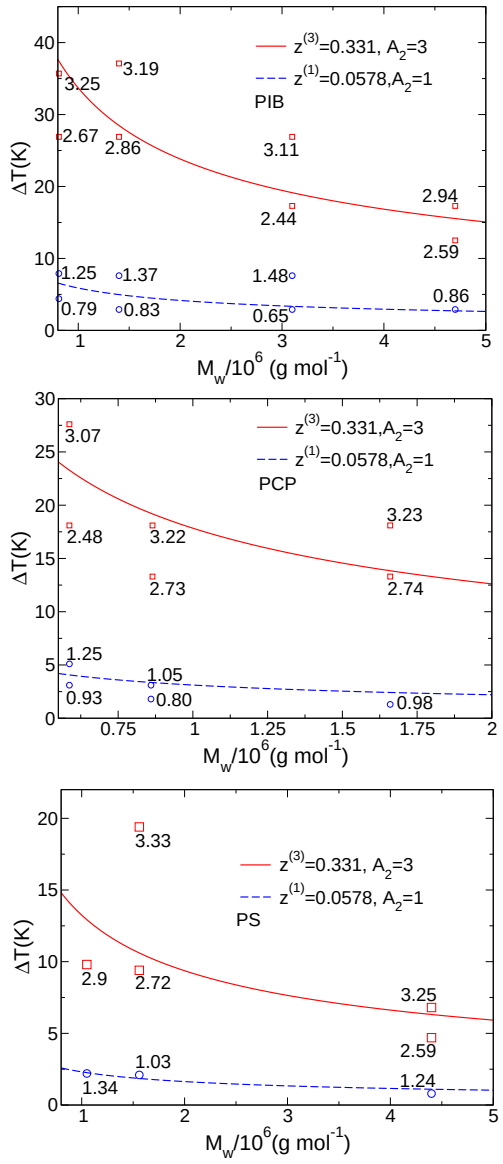

FIG. 1: Thermal crossover for polyisobutylene (PIB) in isoamyl-isovalerate (top), polychloroprene (PCP) in trans-decalin (middle), and polystyrene (PS) in decalin (bottom): Lines $z = z^{(1)}$ (dashed line) and $z = z^{(3)}$ (continuous line) in the plane ($\Delta T = T - T_\theta$, M_w). The variable z is defined in Eq. (1) and the constant $a^{(1)}$ is estimated in the supplementary material.[50] Empty points correspond to the experimental results, taken from Refs. 55–57. The number which is reported close to each point gives the corresponding experimental estimate of $A_{2,pp}$.

lated to the polymer chemical potential μ_p by the polymer equation of state in the absence of colloids:

$$\beta\mu_p(\phi_p^{(r)}) = \beta\mu_p^{\rm id}(\phi_p^{(r)}) + \int_0^{\phi_p^{(r)}} \frac{K_p(\eta_p)-1}{\eta_p} d\eta_p. \quad (11)$$

Here $\mu_p^{\rm id}$ is the ideal-gas contribution, $K_p(\phi_p)$ is the inverse isothermal compressibility,

$$K_p(\phi_p) = \frac{\partial \beta P}{\partial \rho_p}, \quad (12)$$

P is the (osmotic) pressure in the absence of colloids, $\phi_p = V_p\rho_p$, $V_p = 4\pi R_g^3/3$, R_g is the zero-density polymer radius of gyration, and $\beta = 1/k_BT$. In the GFVT one makes the following ansatz for the semigrand potential Ω:[30]

$$\omega(\phi_c, \phi_p^{(r)}) = \frac{V_c}{V}\beta\Omega = f(\phi_c) - \frac{1}{q^3}\int_0^{\phi_p^{(r)}} \alpha[\phi_c, \Delta(\eta_p)] K_p(\eta_p) d\eta_p, \quad (13)$$

where $f(\phi_c) = V_c\beta F_{\rm coll}/V$, $F_{\rm coll}$ is the colloid canonical free energy in the absence of polymers, $\Delta(\eta_p)$ is a function that will be specified below, and $\alpha(\phi_c, d)$ is the so-called free-volume factor for the insertion of a particle of radius $R_p = R_c d$ in a colloidal system at volume fraction ϕ_c. For $f(\phi_c)$ we use the Carnahan-Starling approximation in the fluid phase,[69]

$$f(\phi_c) = \phi_c \log\left(\frac{\phi_c\lambda_c^3}{V_c}\right) - \phi_c + \frac{4\phi_c^2 - 3\phi_c^3}{(1-\phi_c)^2}, \quad (14)$$

where λ_c is the colloid thermal length. In the solid phase we use[33,70]

$$f(\phi_c) = 2.1178\phi_c - 3\phi_c \log\frac{1-\phi_c/\phi_{cp}}{\phi_c} + \phi_c \ln\frac{\lambda_c^3}{V_c}, \quad (15)$$

where $\phi_{cp} = \pi/(3\sqrt{2})$. The pressure derivative $K_p(\phi_p)$ is obtained by using the accurate polymer equation of state reported in Ref. 53 (good-solvent case) and in Ref. 51 (thermal crossover region). They are reported for completeness in the supplementary material.[50] For the free-volume factor we use the expression obtained in the framework of scaled particle theory (SPT),[10,33,71] both in the fluid and solid phases:

$$\alpha(\phi_c, d) = (1-\phi_c)e^{-Q(\phi_c,d)}, \quad (16)$$

with[72]

$$Q(\phi_c, d) = (3d + 3d^2 + d^3)y + (9d^2/2 + 3d^3)y^2 + 3d^3y^3, \quad (17)$$

where $y = \phi_c/(1-\phi_c)$. We have also computed the function $\alpha(\phi_c, d)$ from the equation of state for a bidisperse system of hard spheres of Mansouri *et al.*,[73] obtaining[74]

$$\alpha_{MCSL}(\phi_c, d) = (1-\phi_c)^{(1-d)^2(1+2d)} e^{-Q_{MCSL}(\phi_c,d)}, \quad (18)$$

where

$$Q_{MCSL}(\phi_c, d) = (3d + 6d^2 - d^3)y + (3d^2 + 4d^3)y^2 + 2d^3y^3. \quad (19)$$

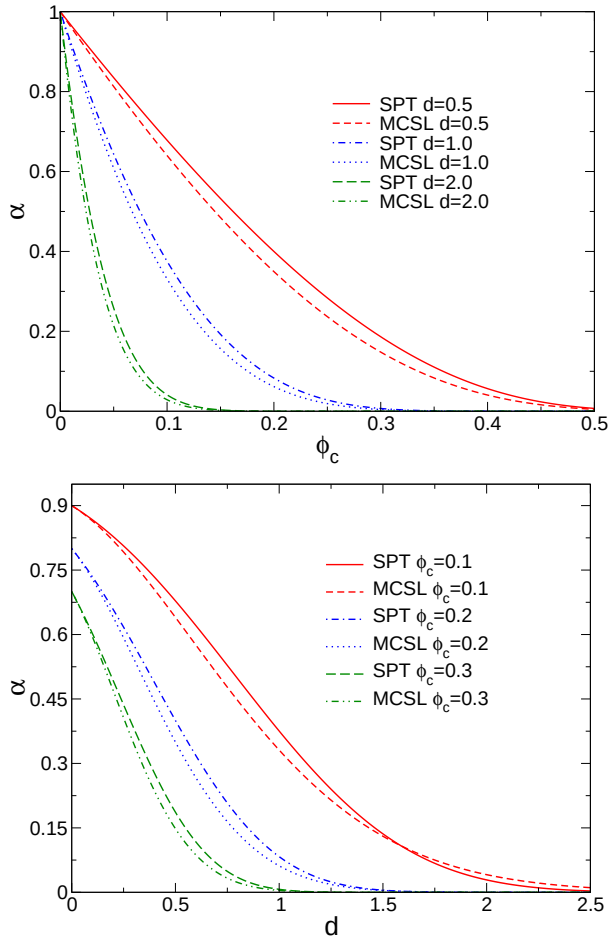

FIG. 2: Plot of $\alpha(\phi_c, d)$ obtained by using SPT and by using the Mansouri *et al.* equation of state (MCSL). In the top panel we plot $\alpha(\phi_c, d)$ versus ϕ_c for three different values of d, in the lower panel we plot it versus d for three values of ϕ_c.

The two expressions (16) and (18) are equivalent for $d \ll 1$ (ϕ_c arbitrary) (in this limit we have $\alpha \approx \alpha_{MCSL} \approx (1-\phi_c)e^{-3dy}$), for $1 \ll d \ll \phi_c^{-1/3}$ ($\alpha \approx \alpha_{MCSL} \approx e^{-d^3\phi_c}$), and for ϕ_c small ($d \ll \phi_c^{-1/3}$) ($\alpha \approx \alpha_{MCSL} \approx 1-(1+d)^3\phi_c$). In general, see Fig. 2, differences are tiny in the relevant region in which $\alpha(\phi_c, d)$ is not too small. For $d \lesssim 2$ and $\phi_c \lesssim 0.6$, differences are small in all cases, making the two expressions equivalent for our purposes. In the following we use Eq. (16). For comparison, some calculations will be repeated using the more accurate expression (18).

Finally, we should specify the function $\Delta(\phi_p)$, which gives the ratio of the effective size of the polymer and the radius of the colloid. We will define it as $\Delta(\phi_p) = \delta_s(q, \phi_p)/R_c$, where $\delta_s(q, \phi_p)$ is the depletion thickness as defined in Refs. 5,33. For such a quantity we use the accurate expressions determined in Ref. 52 and reported for completeness in the supplementary material.[50]

Once ω is known, the pressure and the colloid chemical potential can be computed by using

$$\beta P V_c = \phi_c \left(\frac{\partial \omega}{\partial \phi_c}\right)_{\phi_p^{(r)}} - \omega \qquad \beta\mu_c = V_c \left(\frac{\partial \omega}{\partial \phi_c}\right)_{\phi_p^{(r)}}. \tag{20}$$

The polymer volume fraction ϕ_p can be derived by using

$$\begin{aligned} \phi_p = V_p \rho_p &= -q^3 \frac{\phi_p^{(r)}}{K_p(\phi_p^{(r)})} \frac{\partial \omega}{\partial \phi_p^{(r)}} \\ &= \alpha[\phi_c, \Delta(\phi_p^{(r)})]\phi_p^{(r)}. \end{aligned} \tag{21}$$

B. Comparison with full-monomer data

By construction GFVT provides the exact semigrand potential on the polymer ($\phi_c = 0$) and colloid ($\phi_p^{(r)} = 0$) axis, provided one uses the exact expression for $F_{\rm coll}$ and $K_p(\phi_p)$. Moreover, if one uses an accurate estimate of $\delta_s(q, \phi_p)$ (we remind the reader that the knowledge of $\delta_s(q, \phi_p)$ is equivalent to the knowledge of the insertion free energy of a single colloid in the pure polymer solution), the potential $\omega(\phi_c, \phi_p^{(r)})$ is also accurate close to the polymer axis to first order in ϕ_c. We wish now to study the accuracy of the approximation in the (ϕ_c, ϕ_p) plane, below the phase separation line.

Let us first consider the dilute limit, in which the polymer and colloid densities ρ_p and ρ_c are both small. In this regime the pressure can be expanded as

$$\begin{aligned} \beta P = \rho_c + \rho_p + B_{2,cc}\rho_c^2 + B_{2,pp}\rho_p^2 + B_{2,cp}\rho_c\rho_p \\ + B_{3,ccc}\rho_c^3 + B_{3,ppp}\rho_p^3 + B_{3,ccp}\rho_c^2\rho_p + B_{3,cpp}\rho_c\rho_p^2 + \ldots \end{aligned} \tag{22}$$

The virial coefficients are not universal as they depend on the details of the system. On the other hand, the combinations

$$A_{2,\#} = B_{2,\#} R_g^{-3} \qquad A_{3,\#} = B_{3,\#} R_g^{-6} \tag{23}$$

are model independent in the limit of large degree of polymerization. These combinations have been determined quite accurately in Refs. 52,67,68. If we start from the GFVT semigrand potential (13) we obtain a low-density expansion analogous to Eq. (22), with corresponding coefficients $A_{2,\#}^{(GFVT)}$ and $A_{3,\#}^{(GFVT)}$. If we use accurate estimates for the colloid free energy density $f(\phi_c)$, for the derivative $K_p(\phi_p^{(r)})$, and for the depletion thickness, we have $A_{2,\#}^{(GFVT)} \approx A_{2,\#}$ and

$$\begin{aligned} A_{3,ppp}^{(GFVT)} &\approx A_{3,ppp} \qquad A_{3,ppc}^{(GFVT)} \approx A_{3,ppc} \\ A_{3,ccc}^{(GFVT)} &\approx A_{3,ccc}. \end{aligned} \tag{24}$$

The only virial combination for which the approximate equality does not hold is $A_{3,ccp}$, for which we obtain (see

TABLE I: Estimates of the third virial combination $A_{3,ccp}$ obtained by using GFVT and full-monomer (FM) simulations.

	$q=0.5$		$q=1$		$q=2$	
z	FM	GFVT	FM	GFVT	FM	GFVT
∞	8630(45)	9056	360(2)	403	16.8(1)	20.7
$z^{(3)}$	9300(30)	9788	399(1)	451	19.2(1)	24.2
$z^{(1)}$	9500(30)	10025	409(1)	466	19.6(1)	25.4

Appendix)

$$A_{3,ccp}^{(GFVT)} = \frac{32\pi A_{2,cp}^{(GFVT)}}{3q^3} + \frac{32\pi^2}{9q^6} - 9\left[A_{2,cp}^{(GFVT)}\right]^{2/3}\left(\frac{4\pi}{3q^3}\right)^{4/3}. \quad (25)$$

Since we use the accurate expression of the depletion thickness of Ref. 52, $A_{2,cp}^{(GFVT)} \approx A_{2,cp}$, hence Eq. (25) gives us a prediction which can be compared with the full-monomer result. For $q \to 0$, we have $A_{2,cp} \approx 4\pi/(3q^3)$ for any value of z, so that $A_{3,ccp}^{(GFVT)} \approx 16\pi^2/(9q^6)$ in the same limit, which is indeed the correct small-q limiting behavior.[52] For large values of q, we have $A_{3,ccp}^{(GFVT)} q^3/A_{2,cp}^{(GFVT)} \approx 32\pi/3 \approx 34$, which should be compared with the numerical result $A_{3,ccp}q^3/A_{2,cp} \approx 17$, 21, 15 (these estimates are obtained by using the interpolations reported in Ref. 52) for $z=\infty$, $z^{(3)}$, and $z^{(1)}$. These results indicate that $A_{3,ccp}$ is quite precisely reproduced for $q \to 0$, while discrepancies are expected for large q. We can also make a more detailed check for $q = 0.5, 1$ and 2, comparing the Monte Carlo estimates[52] of $A_{3,ccp}$ and the prediction $A_{3,ccp}^{(GFVT)}$ obtained by using the Monte Carlo estimate[52] of $A_{2,cp}$. The results are reported in Table I. GFVT overstimates $A_{3,ccp}$ by 5%, 13%, 23-30% for $q = 0.5$, 1, and 2. Clearly, the approximation works very well for small values of q and worsens somewhat as q increases. Apparently, the accuracy is also higher for good-solvent conditions than close to the θ point.

To check the accuracy of the GFVT predictions at finite densities, we have performed finite-density simulations of a lattice polymer-colloid system in a finite box of volume V. Polymers are modelled as Domb-Joyce[75] walks of length L on a cubic lattice, while colloids are modelled as hard spheres of radius R_c, whose centers lie in the continuum space. This model, already discussed in D'Adamo *et al.*,[52] allows us to study both the good-solvent regime ($z = +\infty$) and the thermal crossover region. We compare GFVT and full-monomer results for the adimensional combination $\beta R_c^3/\kappa_T$, where κ_T is the isothermal compressibility

$$\kappa_T = -\frac{1}{V}\left(\frac{\partial V}{\partial p}\right)_{N_c,N_p}. \quad (26)$$

TABLE II: Comparison of the isothermal compressibility. We report $\beta R_c^3/\kappa_T$ for $L = 600$ DJ walks in a volume $V = 256^3$ ($L = 600$,FM), the corresponding infinite-volume scaling ($L, V \to \infty$) extrapolation (FM,scal), and the GFVT prediction.

z	q	ϕ_c	ϕ_p	$L=600$,FM	FM,scal	GFVT
∞	1	0.1	0.6	1.05(1)		1.056
		0.2	0.2	0.695(2)	0.73(1)	0.666
		0.3	0.2	1.772(6)		1.625
	2	0.1	1.0	0.481(5)		0.469
		0.2	0.8	0.946(9)		0.892
		0.3	0.2	1.063(3)		0.954
z_3	1	0.3	0.05	0.965(3)	0.98(1)	0.902
	2	0.3	0.1	0.810(10)	0.79(1)	0.853

Such a quantity can be expressed[76,77] in terms of the zero-momentum partial structure factors, quantities that can be easily computed in simulations (see Ref. 52 for a discussion). To obtain a universal, i.e., model independent, prediction, the numerical results must be carefully extrapolated. First, since simulations are performed in a finite box [typically we take $V \approx (15R_g)^3$], we must determine the infinite-volume limit. Second, we must perform an extrapolation in the length L of the chains, taking into account that the leading corrections behave as $L^{-\nu}$, where $\nu = 0.588$ in the good-solvent case and $\nu = 1/2$ in the crossover region (see the supplementary material of Ref. 52 for a careful check of this behavior). To perform these two extrapolations[78] one must obtain results for several values of L and V, which is very CPU-time consuming. We have therefore performed the full analysis only in a few cases. We find that the results corresponding to $L = 600$ and $V = 256^3$ differ at most by 10% from the asymptotic ones, a not too large systematic deviation (note that this conclusion is valid only for our model, since scaling corrections are not universal, i.e., they are system dependent). Therefore, it is possible to perform a meaningful comparison with the GFVT data even by using the $L = 600$ data. The results for a few selected points (they have been chosen to lie close to the GFVT binodal) are reported in Table II. It is evident that the approximation works better for ϕ_c small. Quantitatively, deviations are less than 10% in all cases, confirming the relative accuracy of the approximation in the homogeneous phase for $q \lesssim 2$.

IV. POLYMER-COLLOID PHASE DIAGRAM

A. GFVT results

We wish now to use GFVT to determine the phase diagram for the colloid-polymer system. The colloid volume fractions ϕ_{c1} and ϕ_{c2} of the coexisting phases are obtained by equating pressure and colloid chemical po-

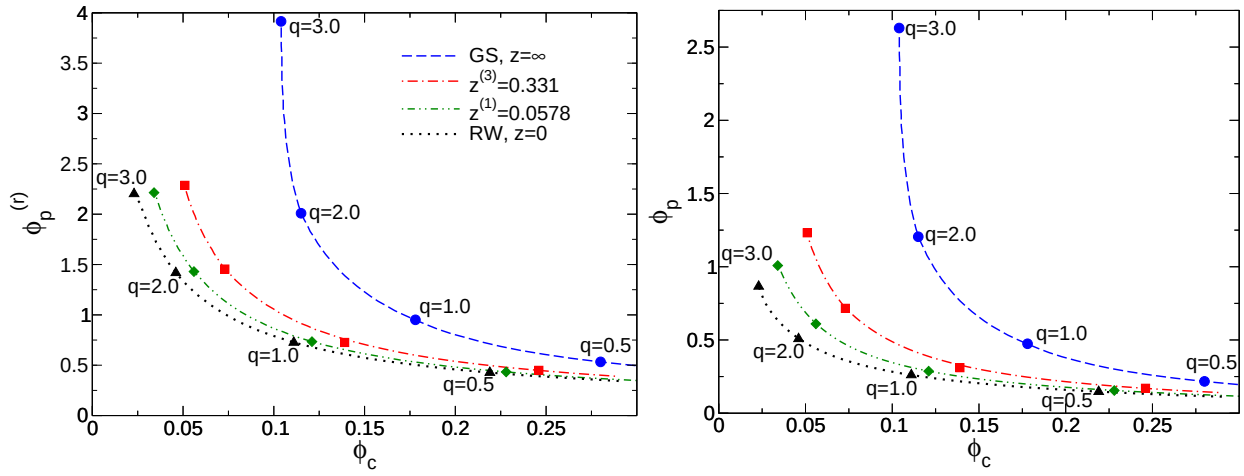

FIG. 3: Critical-point positions in the $\phi_c, \phi_p^{(r)}$ (left) and ϕ_c, ϕ_p (right) planes as q varies between 0.4 and 3. We explicitly report the positions of the critical points corresponding to $q = 0.5,1,2,3$. From top to bottom, the four curves correspond to $z = \infty$ (good-solvent case), $z = z_3$, $z = z_1$, and $z = 0$ (θ conditions).

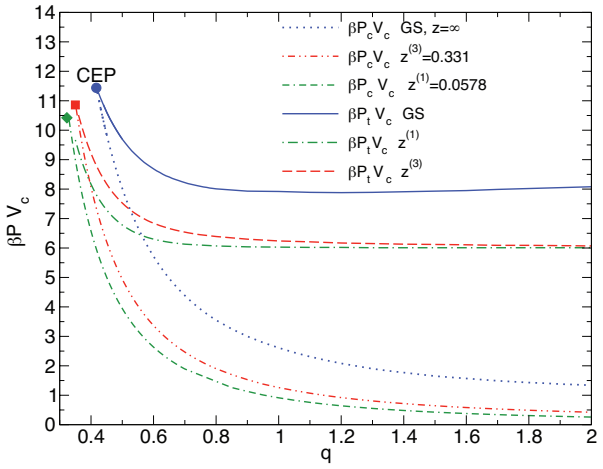

FIG. 4: Critical-point (P_c) and triple-point (P_t) pressure. We report $\widetilde{P} = \beta P V_c$ as a function of q up to the critical endpoint (CEP) for good-solvent (GS) conditions, $z = z^{(3)}$, and $z = z^{(1)}$.

tential at fixed $\phi_p^{(r)}$:

$$P(\phi_{c1}, \phi_p^{(r)}) = P(\phi_{c2}, \phi_p^{(r)}), \quad \mu_c(\phi_{c1}, \phi_p^{(r)}) = \mu_c(\phi_{c2}, \phi_p^{(r)}). \tag{27}$$

As is well known,[33] for small values of q only a solid-fluid transition occurs between a polymer-rich phase in which the colloids are disordered and a colloid crystal phase with a very low density of polymers. As q increases, the phase diagram becomes more complex. For q larger than the critical endpoint value q_{CEP}, beside the solid-liquid transition, the system undergoes a fluid transition (analogous to the liquid-gas transition in simple fluids) between a polymer-rich colloid-poor phase and a polymer-poor colloid-rich phase. The fluid transition is characterized by a critical point, which belongs to the Ising universality class. Moreover, the different phases merge at a triple point, with three coexisting phases. The critical endpoint value q_{CEP} is characterized by the fact that the triple point merges with the critical one.

We will now use GFVT to identify the binodals, the triple and the critical points, as a function of q and for different solvent quality. For the good-solvent case and for noninteracting polymers results have already been presented in Ref. 5,30,33. We will repeat here the same calculation using our more precise expressions for the polymer equation of state and depletion thickness. We anticipate here that differences are small for $q \lesssim 2$, but significantly increase for large values of q, since the phenomenological expression for $\delta_s(q, \phi_p)$ of Ref. 5 becomes inaccurate as q increases beyond 4.[52] We anticipate that such a discrepancy is not very relevant, since GFVT turns out to be not predictive in the protein regime $q > 1$.

We begin by computing the critical endpoint values q_{CEP} for different values of z. We obtain $q_{CEP} \approx 0.42, 0.35, 0.32, 0.31$ for $z = \infty$, z_3, z_1, and for $z = 0$, respectively. Clearly, q_{CEP} depends somewhat on solvent quality—it decreases as one approaches the θ point—but the change is relatively small. If one uses the expressions of K and δ_s reported in Ref. 5,33,79 (see supplementary material[50]), one would obtain $q_{CEP} \approx 0.39$ for the good-solvent case. As anticipated the difference is small.

In Fig. 3 we report the position of the critical points as q varies (an extensive table of results is given in the supplementary material[50]), while in Fig. 4 we report the reduced pressure $\widetilde{P} = \beta P V_c$, at the critical and at the triple point, as a function of q. From the results it is evident that solvent quality is an important variable.

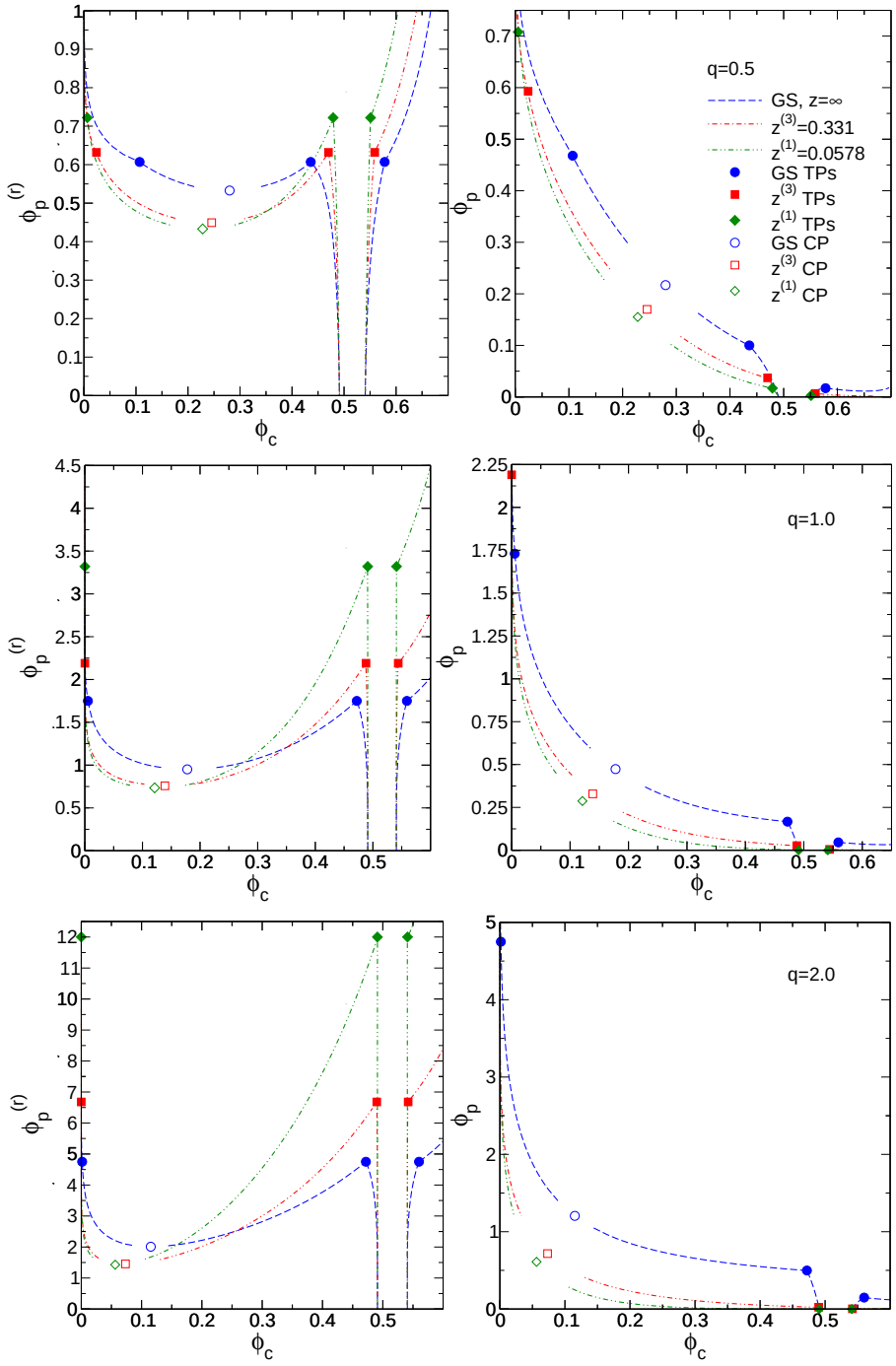

FIG. 5: Binodals as a function of ϕ_c and $\phi_p^{(r)}$ (left) and of ϕ_c and ϕ_p (right). We report data for $q = 0.5$ (top), $q = 1$ (middle), $q = 2$ (bottom). Empty symbols correspond to the critical point (CP), filled symbols label the different phases coexisting at the triple point (TPs).

If z increases, both critical volume fractions $\phi_{c,\mathrm{crit}}$ and $\phi_{p,\mathrm{crit}}$ increase significantly. For $q \gtrsim 2$, $\phi_{c,\mathrm{crit}}$ and $\phi_{p,\mathrm{crit}}$ change approximately by a factor of 2 as z varies between 0 and ∞. Note that the change of the critical point from $z = z^{(3)}$ to the good-solvent regime (which correspond to a change of the second-virial combination $A_{2,pp}$ from 3.0 to 5.5) is larger than that between the θ point and $z = z^{(3)}$ (correspondingly, $A_{2,pp}$ varies between 0 and 3), an indication that phase coexistence is more sensitive to small deviations from the good-solvent regime than to deviations from θ behavior. This is also evident from the binodals reported in Fig. 5. For the

considered values of q, the binodals in the (ϕ_c, ϕ_p) plane for $z = z^{(1)}$ and $z = z^{(3)}$ are very close and significantly lower than the good-solvent ones. We also report the position of the triple points (extensive tables of numerical data are reported in the supplementary material[50]), whose position varies significantly with z. In particular, the polymer volume fractions ϕ_{pl} and ϕ_{ps} in the coexisting liquid and solid phases are very small for $z = z^{(3)}$ and $z = z^{(1)}$ and typically an order of magnitude smaller than in the good-solvent regime. Moreover, the q dependence of these quantities is qualitatively different in the two cases. In the good-solvent case ϕ_{pl} and ϕ_{ps} increase with increasing q (for instance, $\phi_{pl} = 0.167, 0.498$ for $q = 1, 2$ respectively), while in the thermal crossover region the opposite occurs. For instance, for $z = z^{(3)}$ we have $\phi_{pl} = 0.027, 0.023$ for $q = 1, 2$ respectively. We have also determined the pressure. Its value at the critical and triple points is reported in Fig. 4. At the critical endpoint (CEP) the pressure has a small dependence on solvent quality. As q increases, the relative difference between the results for the good-solvent case and for $z = z^{(1)}$, $z^{(3)}$, also increases. For instance, for $q = 2$ we have $\widetilde{P} = \beta P_{\rm crit} V_c = 1.34$ for good-solvent conditions, and $\widetilde{P} = 0.26$ for $z = z^{(1)}$. On the other hand, results for $z = z^{(3)}$ and $z = z^{(1)}$ are always very close.

The results we have discussed have been obtained by using the SPT expression (16) for the free-volume factor. The same calculations can be repeated by using Eq. (18). Differences are tiny in all cases. For instance, for $q = 1$ and good-solvent polymers, we obtain $\phi^{(r)}_{p,\rm crit} = 0.951$, $\phi_{c,\rm crit} = 0.178$, and $\phi_{p,\rm crit} = 0.474$ using the SPT expression and $\phi^{(r)}_{p,\rm crit} = 0.942$, $\phi_{c,\rm crit} = 0.173$, and $\phi_{p,\rm crit} = 0.479$ using Eq. (18). Clearly, the two expressions are equivalent for our purposes.

Let us now determine the GFVT binodals in the protein regime, in which q is large. We will only consider the good-solvent case, in which our results significantly differ from those of Ref. 5. The results presented in Fig. 3 apparently suggest $\phi_{c,\rm crit} \approx 0.10$ as $q \to \infty$. As we now discuss, this is not correct, since, as q increases beyond 2-3, $\delta_s(q, \phi_p)$ shows a crossover[52] to a different, large-q behavior. In particular, general renormalization-group arguments predict[52,80]

$$\frac{\delta_s}{R_c} = \Delta_<(q, \phi_p) = \left(\frac{3A_{\gamma,\infty}}{K_p(\phi_p)}\right)^{1/3} q^{1/3\nu}, \qquad (28)$$

with[52,80] $A_{\gamma,\infty} \approx 1.41$ as long as $R_c \ll \xi \ll R_g$, where ξ is the polymer correlation length. In the opposite case, $R_c \gg \xi$, we have instead[52,81]

$$\frac{\delta_s}{R_c} = \Delta_>(q, \phi_p) = 0.649 q \phi_p^{-\gamma}, \qquad (29)$$

where

$$\gamma = \frac{\nu}{3\nu - 1} \approx 0.7703. \qquad (30)$$

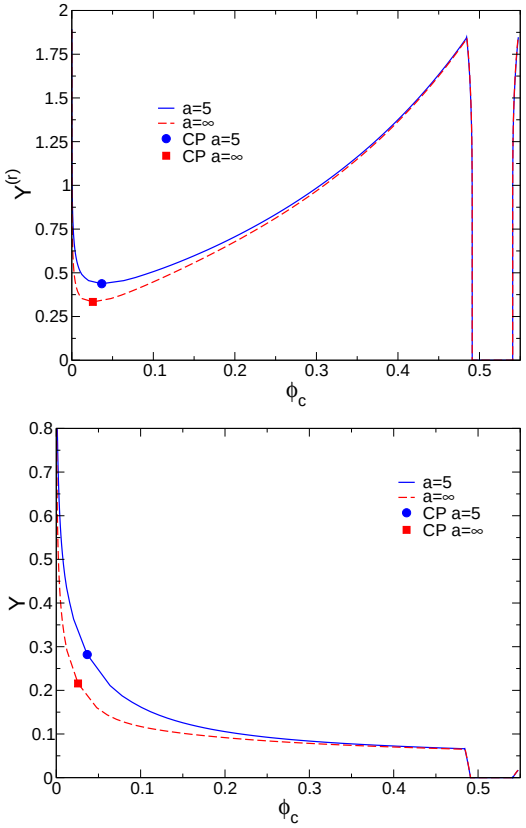

FIG. 6: Universal large-q binodals as a function of ϕ_c and $Y^{(r)}$ (top) and of ϕ_c and Y (bottom).

As discussed in Ref. 40, in the protein limit $q \to \infty$ a universal scaling behavior is observed provided one uses

$$Y_q = \phi_p q^{-1/\gamma} \qquad (31)$$

as basic scaling variable. Indeed, phase separation occurs deep in the semidilute regime for large values of q. The relevant length scale is therefore the correlation length ξ and the relevant adimensional volume fraction is proportional to $\rho_p \xi^3$, which, in turn, is proportional to Y_q, since[82] $\xi \sim R_g(\phi_p = 0)\phi_p^{-\gamma}$. The GFVT binodals show this universal scaling behavior[5] for large q. Hence, for large q one finds

$$\phi^{(r)}_{p,\rm crit} q^{-1/\gamma} \approx Y^{(r)}_{c,\infty}, \qquad \phi_{p,\rm crit} q^{-1/\gamma} \approx Y_{c,\infty}, \qquad (32)$$

while $\phi_{c,\rm crit}$ and $\widetilde{P} = \beta P V_c$ converge to constants $\phi_{c,c,\infty}$ and $\widetilde{P}_{c,\infty}$. To estimate these quantities, we must have an expression for δ_s/R_c which is valid for large q and all values of ϕ_p and which, therefore, interpolates between the two expressions (28) and (29). We have used two different interpolants, in order to be able to estimate roughly how important the interpolation is. We consider the family of

TABLE III: Large-q critical and triple points. The subscript c refers to the critical point, t to the triple point, tg, tl, and ts refer to the three phases (gas, liquid, solid) coexisting at the triple point. We report results corresponding to two different interpolations for δ_s/R_c ($a = 5$ and $a = \infty$) and the results (FT) of Ref. 5.

	$a = 5$	$a = \infty$	FT
Critical point			
$\phi_{c,c,\infty}$	0.037	0.025	0.104
$Y^{(r)}_{c,\infty}$	0.440	0.337	0.97
$Y_{c,\infty}$	0.296	0.218	0.665
$\widetilde{P}_{c,\infty}$	0.25	0.13	0.360
Triple point			
$\phi_{c,tg,\infty}$	$2 \cdot 10^{-4}$	$2 \cdot 10^{-4}$	0
$\phi_{c,tl,\infty}$	0.484	0.485	0.469
$\phi_{c,ts,\infty}$	0.548	0.547	0.565
$Y^{(r)}_{t,\infty}$	1.85	1.84	2.08
$Y_{tg,\infty}$	1.85	1.85	2.08
$Y_{tl,\infty}$	0.068	0.065	0.25
$Y_{ts,\infty}$	0.018	0.017	0.09
$\widetilde{P}_{t,\infty}$	6.61	6.58	8.82

interpolants

$$\frac{\delta_s(q,\phi_p)}{R_c} = \left[\Delta_<(q,\phi_p)^{-a} + \Delta_>(q,\phi_p)^{-a}\right]^{-1/a}, \quad (33)$$

which depend on the parameter $a > 0$. In the following we quote results for $a = 5$ and $a = \infty$, the latter choice corresponding to

$$\frac{\delta_s(q,\phi_p)}{R_c} = \min\left[\Delta_<(q,\phi_p), \Delta_>(q,\phi_p)\right]. \quad (34)$$

The results for the critical and the triple point are reported in Table III.

The results for the critical point depend significantly on the chosen interpolation, indicating how crucial the expression for $\delta_s(q,\phi_p)$ is in estimating the critical point. Note also that $\phi_{c,c,\infty}$ and $\widetilde{P}_{c,\infty}$ differ significantly from the values that would have been guessed by looking at Figs. 3 and 4, implying a significant crossover as q increases beyond 3. These results differ from those of Ref. 5, as their expression for δ_s/R_c does not have the correct behavior for q large and $R_c \lesssim \xi$.[52] In Fig. 6 we report the large-q binodals as a function of Y and ϕ_c. The curve shows a significant dependence on the interpolation close to the critical point. However, differences decrease as one moves away from the critical point towards the triple point.

TABLE IV: Critical-point position and pressure ($\widetilde{P} = \beta P V_c$) from full-monomer simulations of a lattice colloid-polymer system (They are obtained by using the results reported in the supplementary material of Ref. 42). The polymer volume fraction has been determined using $R_g = 0.508 L^\nu$, where L is the length of the chain. "extr" gives the extrapolation $L \to \infty$, obtained as discussed in the text.

q	L	$\phi_{c,\rm crit}$	$\phi_{p,\rm crit}$	$\widetilde{P}_{\rm crit}$
1	10	0.146	0.279	1.32
	33	0.186	0.438	2.65
	110	0.202	0.521	3.33
	extr	0.22	0.62	4.15
	GFVT	0.178	0.474	2.61
2	33	0.120	0.537	0.64
	110	0.162	0.770	1.27
	350	0.176	0.905	1.55
	extr	0.19	1.076	1.88
	GFVT	0.115	1.205	1.34
4	110	0.104	1.069	0.37
	350	0.148	1.383	0.70
	extr	0.20	1.78	1.13

B. Comparison with previous work

Let us now compare our results with those appearing in the literature. We have first verified that our results for $z = 0$ (ideal polymers) are in agreement with those obtained in similar studies (we have considered Ref. 12, which gives results for $q = 0.6$ and 0.8). It is also interesting to compare with the results for the AOV model. For $q = 0.8$ simulations give[18,19] $\phi^{(r)}_{p,\rm crit} = 0.766(2)$, $\phi_{p,\rm crit} = 0.3562(6)$, and $\phi_{c,\rm crit} = 0.1340(6)$ for the critical point, to be compared with the free-volume theory predictions $\phi^{(r)}_{p,\rm crit} \approx 0.602$, $\phi_{p,\rm crit} = 0.214$, $\phi_{c,\rm crit} = 0.141$. Analogously, for $q = 1$, one finds[15] $\phi^{(r)}_{p,\rm crit} \approx 0.7$ in the AOV model and $\phi^{(r)}_{p,\rm crit} \approx 0.73$ by using free volume theory. Also the triple-point position is quite accurately predicted: both theories give $\phi^{(r)}_{p,t} \approx 6.0$ for $q = 1$. Clearly, free volume theory provides a good description of the AOV model.

Let us now consider the good-solvent case, for which we can compare with full-monomer results.[40–43] Given the computational complexity of these systems, the simulated chains are typically relatively short and the results show significant corrections to scaling, which should be taken into account before comparing them with our GFVT results. Indeed, the GFVT estimates have been obtained by using the universal asymptotic predictions for $K_p(\phi_p)$ and $\delta_s(q,\phi_p)$, hence they apply to polymer systems in the scaling limit (large degree of polymerization). Ref. 42 reports results for several chain lengths L and several values of q. The critical point position

and pressure are reported in Table IV. To compute the polymer volume fraction we used $R_g = 0.508 L^{\nu}$.[42] Note that scaling corrections are very large in all cases: as L increases, there is a systematic drift of the critical parameters. We expect two types of scaling corrections. First, there are corrections that scale as $L^{-\Delta}$, $\Delta = 0.528(12)$,[62] as in all polymer systems. In the presence of colloids, a second type of corrections appear, related with the renormalization-group operators associated with the colloid-polymer interactions.[52] They scale as $L^{-\nu}$, where $\nu \approx 0.5876$ is the Flory exponent. The two exponents are very close, hence we have extrapolated the finite-length results as $a + bL^{-1/2}$. In Table IV lines labelled "extr" report the corresponding coefficient a. It is important to note that both types of corrections are not related to the lattice breaking of rotational invariance,[83] hence they are present both in lattice and continuum models. Extrapolations for $q = 4$ should not be taken too seriously, given the very large difference between the data and the extrapolation results. In any case, they are roughly consistent with the results of Ref. 40. They studied self-avoiding lattice walks with $L = 2000$ monomers, finding $\phi_{c,\rm crit} \approx 0.24$ and $\phi_{p,\rm crit} \approx 1.9$ for $q = 3.86$. No extrapolation can be done here, hence these results are affected by scaling corrections, which are particularly large for SAWs in the semidilute regime.[53] Still, they confirm that $\phi_{c,\rm crit} \gtrsim 0.20$ and $\phi_{p,\rm crit} \gtrsim 1.8$ for $q \approx 4$. Ref. 40 also presents results for $q = 5.58$ and 7.78. In all cases, they obtain $\phi_{c,\rm crit} \approx 0.25$.

For $q = 1$, the GFVT estimates of $\phi_{c,\rm crit}$ and $\phi_{p,\rm crit}$ both underestimate the extrapolated full-monomer values, differences being of the order of 20-25%, while the pressure is largely underestimated. For $q = 2$, $\phi_{c,\rm crit}$ and $\widetilde{P}_{\rm crit}$ differ by a factor of 2 and 0.5, respectively, from the numerical result, while $\phi_{p,\rm crit}$ is in reasonable agreement. For larger values of q, differences are expected to increase. While numerical data indicate $\phi_{c,\rm crit} \gtrsim 0.20$, GFVT predicts $\phi_{c,\rm crit}$ to converge to 0.02-0.03 as $q \to \infty$. These results show that GFVT looses predictivity in the protein limit. This is not so surprising, since the theory describes polymers as spheres which move in the free space left by the colloids. For $q > 1$, this picture is clearly unrealistic.

Most of the other predictions for the good-solvent case are obtained by studying coarse-grained models in which each polymer is replaced by a monoatomic molecule, as in the AOV model. Ref. 14 uses an exact coarse-graining procedure, which provides density-dependent effective potentials that accurately reproduce pair correlation functions as measured in full-monomer simulations. Monte Carlo studies of the resulting model provide accurate estimates of the critical and of the triple point. The estimates of the critical-point location $(\phi_{c,\rm crit}, \phi_{p,\rm crit}) = (0.19, 0.40)$ and $(0.18, 0.51)$ for $q = 0.67$ and 1.05 are close to the GFVT predictions $(0.23, 0.29)$ and $(0.17, 0.50)$, respectively. The very good agreement for $q = 1.05$, however, is probably accidental and should not be taken too seriously, given that full-monomer simulations, see Table IV, predict $(0.22, 0.62)$ for $q \approx 1$. The reservoir polymer volume fraction at the triple point $\phi_{p,t}^{(r)}$ is also close to the GFVT estimate. The coarse-grained model gives $\phi_{p,t}^{(r)} = 0.90$, 1.62 (for $q = 0.67, 1.05$, respectively) to be compared with 0.97, 1.88 obtained using GFVT. Again, discrepancies increase with q.

There are also results for several coarse-grained phenomenological models. However, in all these cases it is not obvious that they are really appropriate to describe polymers under good-solvent conditions interacting with hard-sphere colloids. Ref. 25 studied a simple model which reproduces the polymer thermodynamics for $\phi_c \to 0$ and provides the correct second-virial combination $A_{2,cp}$. They obtained $\phi_{c,\rm crit} = 0.22$, $\phi_{p,\rm crit} = 0.93(2)$, and $\phi_{p,\rm crit}^{(r)} = 1.321(4)$. While $\phi_{c,\rm crit}$ is in reasonable agreement with the full-monomer results, the polymer volume fraction is too large: since $\phi_{p,\rm crit}$ increases with q, we would expect $\phi_{p,\rm crit} \lesssim 0.6$ for $q = 0.8$. Clearly, this coarse-grained model is not so good as the one discussed in Ref. 14 which uses density-dependent accurate pair potentials. A different model is presented in Refs. 27–29. It reproduces[84] the second-virial combination $A_{2,pp}$ and also the combination $A_{2,cp}$ is in good agreement with the the full-monomer results of Ref. 52. For $q = 0.5$ and 1, the coarse-grained model gives $A_{2,cp} = 109.4$, 29.3 to be compared with the full-monomer results 107.4(3) and 27.54(6). However, the results for $q = 0.56$ show[29] the unexpected feature that the good-solvent binodal is very close to the AOV binodal. This type of behavior is not in agreement with the results of Ref. 14 and with the good-solvent GFVT predictions. This discussion shows that it is not enough to correctly reproduce the thermodynamic behavior of the systems in the dilute regime, a property that the models of Ref. 25 and of Refs. 27–29 both share. An accurate parametrization of the effective potential appears to be a necessary condition to obtain reasonably accurate predictions of the phase diagram.

Finally, let us discuss the results of Refs. 22,24, which consider two different models of interacting polymers. If we compare the critical-point positions they obtain with the good-solvent GFVT predictions, we observe significant differences, much larger than those observed when comparing GFVT results with full-monomer data. As we now discuss, these differences are due to the fact that these models are not appropriate to describe good-solvent polymers, hence their results should not be compared with the corresponding good-solvent GFVT results. For instance, if we consider the model of Ref. 22—the interacting model with $\beta\epsilon = 0.25$—we obtain for the polymer-polymer second virial combination, $A_{2,pp} \approx 3.71$. Therefore, the model describes polymers in the thermal crossover region and the numerical results should rather be compared with the GFVT ones for $z = z^{(3)}$. For $q = 1$, they obtain $\phi_{c,\rm crit} \approx 0.14$, $\phi_{p,\rm crit} \approx 0.2$, which are not far from the GFVT results $\phi_{c,\rm crit} \approx 0.139$, $\phi_{p,\rm crit} \approx 0.329$ for $z = z^{(3)}$. Discrepancies are significantly reduced. Also the model of Ref. 24 does not

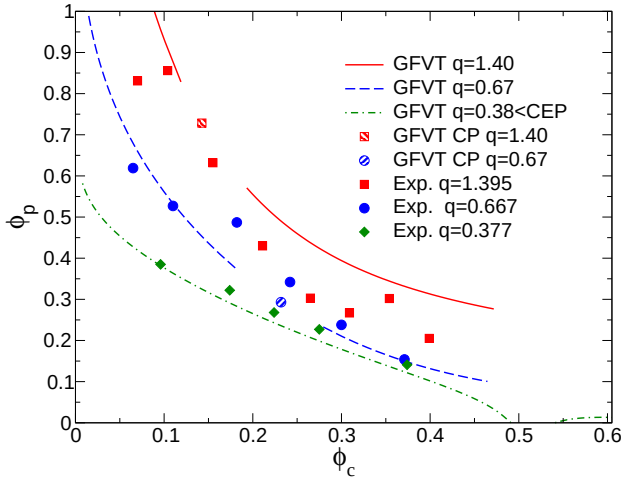

FIG. 7: Comparison of the experimental data of Ref. 36 with the good-solvent GFVT predictions.

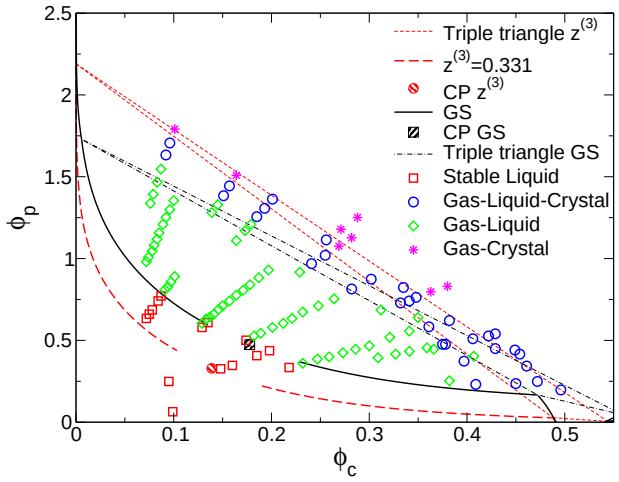

FIG. 8: Comparison of the experimental data of Ref. 32 for a solution of poly-methylmethacrylate colloids and linear polystyrene in a mixture of cis-decalin and tetralin with the GFVT predictions. We report the GFVT binodal, critical point, and triple-point triangle for $z = z^{(3)}$ and $z = \infty$. We use $q = 0.95$. Symbols correspond to the experimental data.

appear to describe good-solvent polymers. As noted in Ref. 25, $A_{2,pp} = 1.78$, hence the results should be better compared with those appropriate for $z = z^{(1)}$. With this identification, the Monte Carlo results are close to the GFVT ones.

Finally, it is interesting to compare GFVT with experiments. An extensive discussion of experiments is reported in Ref. 5. Here we will only make a few comments on the most recent ones. A solution of polystyrene in toluene at 35°C, which is a well-known example of good-solvent system,[85,86] mixed with silica particles was studied in Ref. 36. The experimental results were compared (see their figure 5) with the original version of free-volume theory (appropriate for θ-point solutions), observing large discrepancies. Here we perform the same comparison with GFVT, see Fig. 7. We observe a relatively good agreement for $q = 0.337$ (which is below the critical endpoint) and for $q = 0.667$. Discrepancies are observed instead for $q = 1.395$, confirming again that GFVT is reasonably accurate in the colloid regime, but becomes unreliable as q increases beyond 1. In Ref. 36 the experimental results are also compared with PRISM predictions.[34,35] A comparison of their Fig. 8 with our Fig. 7 shows that PRISM is significantly less accurate than GFVT.

Finally, let us consider the experimental results of Ref. 32. They consider poly-methylmethacrylate colloids and linear polystyrene in a mixture of cis-decalin and tetralin. Assuming that the addition of tetralin does not change the properties of the solution as argued by Tuinier *et al.*,[32] the results presented in the supplementary material for linear polystyrene give $z = 0.30$-0.35 for a polymer of molar weight $15.4 \cdot 10^6$ g/mol and for $T - T_\theta = 3\,\mathrm{K}$. Since $z^{(3)} \approx 0.32$, the solution should not be considered as a good-solvent system, but rather as a system in the thermal crossover region. Using Eq. (9) we predict $\alpha_g = 1.12$ and $R_g = 123$ nm, so that $q = 0.95$ ($R_c \approx 130$ nm). Therefore, the experimental data should be compared with the GFVT results for $z = z^{(3)}$, rather then with those appropriate for good-solvent systems. In Fig. 8 we compare theory and experiments. It is evident that GFVT for the appropriate value of z underestimates the experimental binodal, as already observed when comparing theory and numerical data at $q \approx 1$. On the other hand, the triple-point triangle obtained by GFVT for $z = z^{(3)}$ appears to be in better agremement with the experiment than that obtained by considering good-solvent conditions.

The large-q phase diagram was investigated by Mutch *et al.*,[87–89] considering water-in-oil microemulsion droplets mixed with polyisoprene in cyclohexane, which is an approximately good-solvent system.[90] For the colloid critical volume fraction, they quote[88] $\phi_{c,\mathrm{crit}} = 0.21$ for $q = 4, 10$ and $\phi_{c,\mathrm{crit}} = 0.19$ for $q = 16$. It is quite clear that $\phi_{c,\mathrm{crit}}$ is much larger than the GFVT prediction, which is clearly not reliable for large q. On the other hand, they are close to the numerical full-monomer estimates given in Table IV, provided that the extrapolation to the scaling limit is performed. They are also reasonably consistent with the estimates of Ref. 40. The expected large-q scaling as a function of ϕ_c and $\phi_p q^{-1/\gamma}$ was also tested. Reasonable agreement was observed, although small differences were observed for $\phi_c \gtrsim 0.2$. These differences are probably a consequence of the fact that polyisoprene is not exactly a good-solvent system for the considered values of M_w. For instance, in the range of masses considered in Ref. 91, the gyration radius scales as $M_w^{0.545}$ and not as $M_w^{0.5876}$. Note also that the best estimate of $A_{2,pp}$ for the sample considered in Ref. 88 is[90] $A_{2,pp} \approx 4.80$, which is somewhat less than the

TABLE V: Charged-colloid systems: Critical endpoint values q_{CEP} for $z = 0$ (RW), $z = z^{(1)}$, $z^{(3)}$, and for good-solvent (GS) polymers, as a function of s.

s	RW	$z^{(1)}$	$z^{(3)}$	GS
1.00	0.31	0.32	0.35	0.42
1.01	0.32	0.33	0.36	0.44
1.02	0.33	0.35	0.38	0.46
1.03	0.34	0.36	0.40	0.49
1.04	0.35	0.37	0.41	0.52
1.05	0.37	0.39	0.43	0.55
1.06	0.38	0.40	0.45	0.59
1.07	0.40	0.42	0.48	0.63

good-solvent value[67] 5.50. A second possible reason for the discrepancy is colloid polydispersity, which appears to increase with the size of the colloids.

V. GENERALIZATION TO CHARGED-COLLOID SYSTEMS

In the previous Sections we considered dispersions of hard-sphere colloids and nonadsorbing neutral polymer chains. However, in many practical applications colloids cannot be modelled as hard spheres, since their interaction is characterized by an additional repulsive tail. For instance, this is the case of charged colloids in an aqueous salt solution, in which the effective colloid-colloid potential presents a Yukawa-like tail that depends on temperature, on the dielectric constant, and on the salt concentration of the solvent. GFVT has been generalized to this class of systems[54,92,93] and, more generally, to systems in which the colloid-colloid interaction presents an additional repulsive tail. As before, polymers are modelled as soft spheres of radius $\delta_s(q, \phi_p)$ interacting with colloids of radius R_c. To keep into account the Yukawa tail in the colloid-colloid interaction, the colloid potential is taken as

$$\begin{aligned} U &= +\infty \qquad |\mathbf{r}_{1,c} - \mathbf{r}_{2,c}| \le 2sR_c, \\ U &= 0 \qquad\quad |\mathbf{r}_{1,c} - \mathbf{r}_{2,c}| > 2sR_c, \end{aligned} \tag{35}$$

where s is a parameter, which can be related to the original potential by using the Barker-Henderson relation.[94] For $s = 1$ we reobtain the hard-sphere potential, while the additional repulsive tail is mimicked by taking $s > 1$. As before, we define $q = R_g/R_c$, $V_c = 4\pi R_c^3/3$, and $\phi_c = V_c\rho_c$, where ρ_c is the colloid number density. Note that, with these definitions, the colloid fluid phase ends at $\phi_c \approx 0.49/s^3$ for $\phi_p \to 0$. To generalize the GFVT potential to this nonadditive system, two changes should be made.[54] First, we must modify the colloid zero-polymer-density contribution to $\omega(\phi_c, \phi_p^{(r)})$. The function $f(\phi_c)$ given in Eq. (14) should be replaced by $f(s^3\phi_c)/s^3$, to take into account the different interaction range of the potential. The same change should be made on the free energy in the solid phase, see Eq. (15). Second, we should modify the free-volume factor, which takes the form (16) with[54]

$$\begin{aligned} Q(\phi_c, d, s) = \\ (3d + 3d^2)y + 9d^2/2y^2 + d^3y_s(1 + 3y_s + 3y_s^2), \end{aligned} \tag{36}$$

where $y = \phi_c/(1 - \phi_c)$ and $y_s = s^3\phi_c/(1 - s^3\phi_c)$.

Using these expressions, we have repeated the calculations presented in Refs. 54,92 for the ideal and the good-solvent case, and, moreover, we have extended the calculation to the thermal crossover region. We consider values of s in the range $1 \le s \lesssim 1.07$, corresponding to $1 \le m = s^3 \lesssim 1.2$, which is the expected range of validity of the approximation.[93] We have first computed the values q_{CEP} of the critical endpoints which determine the end of the fluid-fluid coexistence region. The results are reported in Table V. The results for the ideal case ($z = 0$) should not agree with those reported in Table 1 of Ref. 92 for the θ case. Indeed, Ref. 92 takes into account the logarithmic corrections to the equation of state, that are present at the θ point. Such corrections are neglected here. The two approaches give similar results for neutral colloids. On the other hand, in the charged case, results differ, discrepancies increasing with increasing s. For instance, for $s = 1.07$ (corresponding to $m = s^3 = 1.225$) we obtain $q_{CEP} = 0.40$ to be compared with the result of Ref. 92, that quotes $q_{CEP} = 0.49$. In any case, the qualitative conclusions of Ref. 92 are always in agreement with ours, and no appreciable differences can be observed by comparing the graphs reported in Refs. 54,92 with those obtained here. In the good-solvent case, in spite of the different expressions used for the depletion thickness and the polymer compressibility factor, our results for q_{CEP} are fully consistent with those of Ref. 92. For instance, for $s = 1.07$ we obtain $q_{CEP} = 0.63$ to be compared with the result of Ref. 92, quoting $q_{CEP} = 0.61$. It is interesting to compare also the results in the crossover region. For $z = z^{(1)}$ q_{CEP} is very close to the value obtained in the ideal case. Apparently, in a large temperature interval around T_θ, the phase diagram changes only slightly. On the other hand, q_{CEP} varies significantly for $z > z^{(3)}$, indicating that the phase diagram is quite sensitive to solvent quality close to the good-solvent regime, as already observed for neutral colloids.

In Fig. 9 we report the volume fractions $\phi_{c,\mathrm{crit}}$, $\phi_{p,\mathrm{crit}}^{(r)}$, and $\phi_{p,\mathrm{crit}}$ corresponding to the critical point for good-solvent and θ conditions. The colloid $\phi_{c,\mathrm{crit}}$ shows a very tiny dependence on s. Solvent quality is here much more important that charge effects. In the θ region, also $\phi_{p,\mathrm{crit}}$ shows a relatively small dependence on s, which furthermore decreases as q is increased. On the other hand, charge effects are important in the good-solvent regime. In particular, the difference between $\phi_{p,\mathrm{crit}}$ in the good-solvent and in the θ regime increases with s, indicating that a careful control of the quality of the solution is

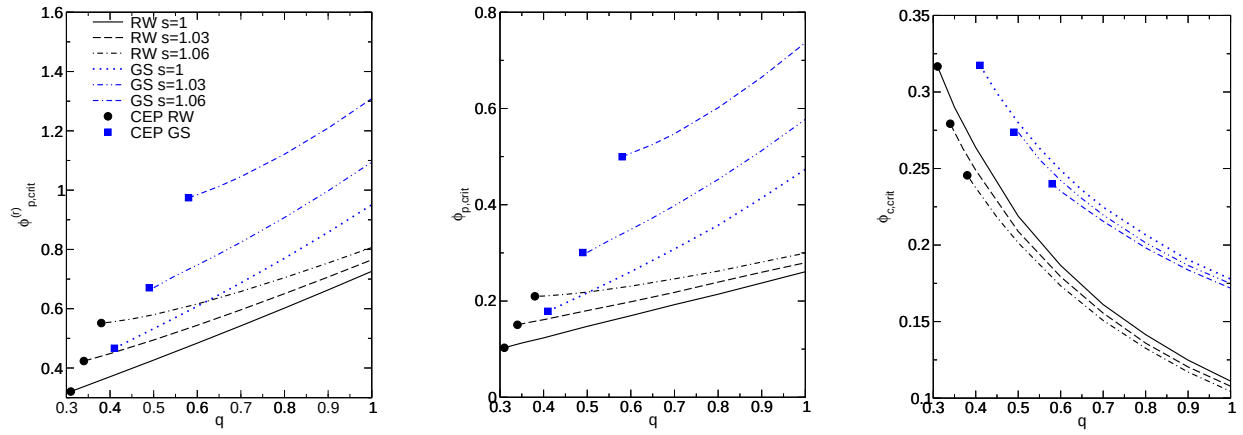

FIG. 9: Fluid-fluid critical-point volume fractions $\phi^{(r)}_{p,\rm crit}$ (left), $\phi_{p,\rm crit}$ (middle), and $\phi_{c,\rm crit}$ (right) as a function of q for different values of the parameter s, for good-solvent (GS) and θ (RW) conditions.

crucial to understand experimental results for charged systems. In the intermediate thermal crossover region, we observe the same phenomenon discussed before. For $z = z^{(1)}$ and also, although to a lesser extent, for $z = z^{(3)}$, $\phi_{p,\rm crit}$ shows a relatively small dependence on s, indicating that charge effects play a relatively small role in a large z (i.e., temperature) interval around θ conditions. They become important only when one approaches the good-solvent region.

In Fig. 10 we report the binodals for the good-solvent case for $s = 1$, 1.03, 1.06 as a function of $s^3\phi_c$ (this guarantees that all binodals converge to the same values as $\phi_p \to 0$). As already discussed in Ref. 92, charge effects are large, moving the binodals towards larger values of ϕ_p. Note that, for $q = 0.5$, liquid-gas coexistence disappears as s is increased. In Fig. 11 we report the binodals for $s = 1.06$, for different solvent quality. As already discussed, the θ binodal and those for $z = z^{(1)}$ and $z = z^{(3)}$ are close, indicating that quality of the solution plays here a minor role, in spite of the fact that thermodynamic dilute properties vary significantly. On the other hand, significant changes occur when the system is close to the good-solvent regime.

VI. CONCLUSIONS

In this paper we studied phase coexistence for dispersions of spherical colloids and neutral polymers. We use an approximate scheme, known as generalized free-volume theory (GFVT),[5,30,31,33] that models polymers as soft spheres with a density-dependent radius identified with the so-called depletion thickness.[33] This approach has already been applied[5] to good-solvent and θ polymers and is extended here to the thermal crossover region between these two regimes.

First, we investigate the good-solvent behavior, using the accurate expressions for the polymer equation of state and for the depletion thickness of Refs. 51–53. For $q \lesssim 1$, our results are in full agreement with those presented in Ref. 5, in which slightly different expressions for the polymer properties were used. On the other hand, our GFVT results differ significantly from those of Ref. 5 in the protein limit $q \gg 1$. This is due to the fact that their expression for the depletion thickness becomes inaccurate for $q \gtrsim 4$.[52] In any case, comparison with full-monomer Monte Carlo data[40,42] and with experiments[87–89] shows that GFVT is not predictive for $q \gtrsim 1$. This is not unexpected, since GFVT models polymers as soft spheres, an approximation that should be reasonably accurate only for $q \lesssim 1$. Note that the comparison with full-monomer results is not straightforward, as the GFVT results refer to polymers in the scaling regime, while simulation are limited to relatively short chains. Hence, a careful extrapolation of the Monte Carlo data is needed before making any comparison.

We also investigate the phase diagram in terms of the crossover variable z. We find that phase behavior is not very sensitive to solvent quality close to the θ point. If we parametrize the thermal crossover in terms of the adimensional ratio $A_{2,pp}$ [or, equivalently, in terms of the interpenetration ratio $\Psi = A_{2,pp}/(4\pi^{3/2})$], we find that binodals and critical points do not change significantly as $A_{2,pp}$ changes from 0 to $0.2A_{2,pp,GS}$, where $A_{2,pp,GS}$ is the value under good-solvent conditions. If $A_{2,pp}$ is increased further, for instance by increasing temperature, we observe a systematic drift of the binodals towards larger values of ϕ_p. Note, however, that in the range $A_{2,pp}/A_{2,pp,GS} \lesssim 0.6$ changes are rather small. Apparently, the phase diagram is very sensitive to solvent quality only close to the good-solvent regime.

Finally, we investigate the phase diagram for charged colloids in an aqueous salt solution. We use here a generalization of GFVT developed in Refs. 54,92. For $z \lesssim z^{(3)}$, the additional repulsion between the charged colloids changes only slightly the phase diagram. On the

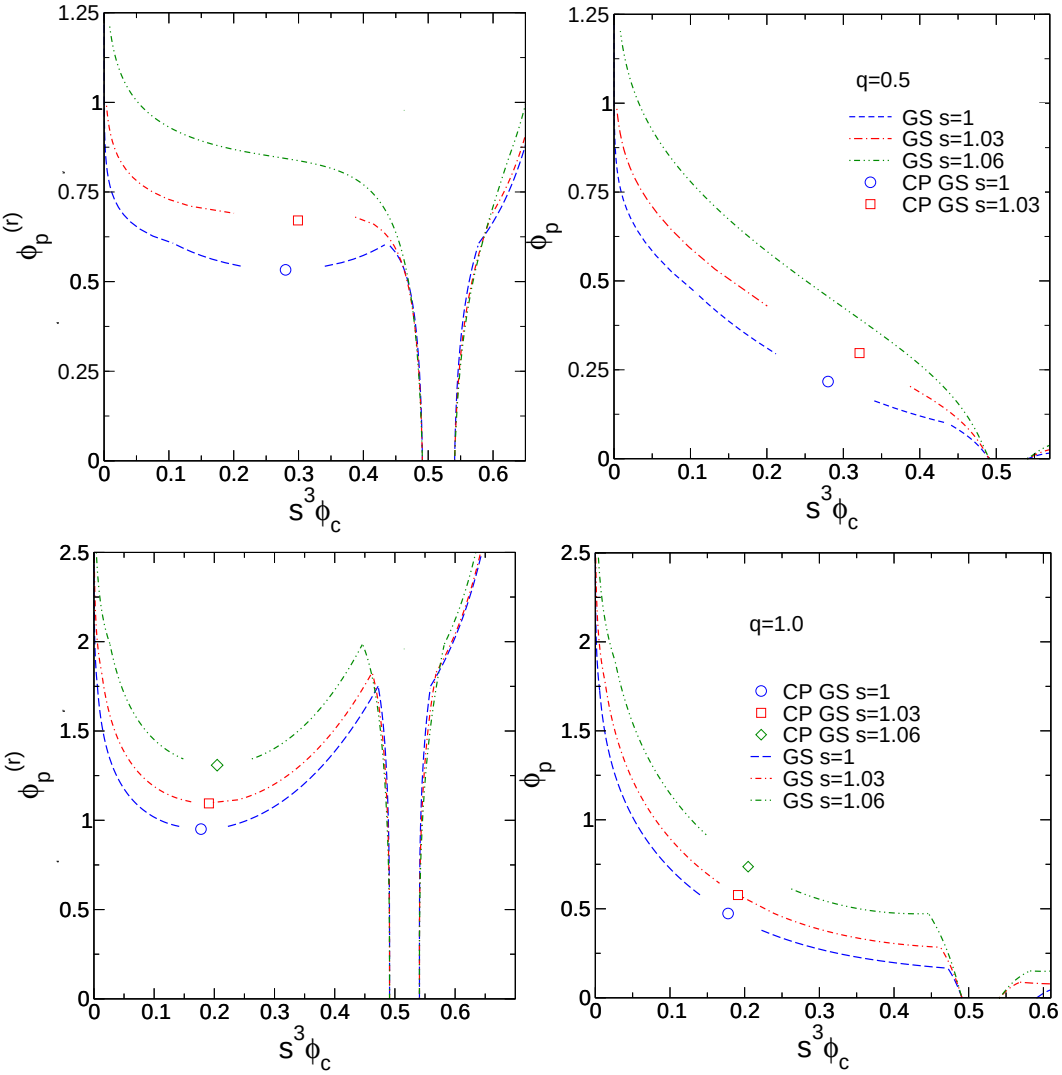

FIG. 10: Binodals and critical points (CP) for good-solvent conditions for several values of s. On the left we report $\phi_p^{(r)}$ and on the right ϕ_p as a function of $s^3\phi_c$. The upper panels refer to $q = 0.5$, the lower ones to $q = 1$. No fluid-fluid transition occurs for $q = 0.5$ and $s = 1.06$.

other hand, close to the good-solvent region, phase behavior shows a strong dependence both on solvent quality and on the parameter s that parametrizes the charge effects. Clearly, a meaningful comparison of experimental results with theory requires a careful determination of the solvent quality, i.e., the swelling ratio α or the second-virial combination $A_{2,pp}$, as discussed in the supplementary material,[50] as well as of the electric properties, i.e. Bjerrum and Debye screening length, colloid charge, etc., of the solution.

Acknowledgments

We thank Profs. Rubinstein and Colby for useful correspondence and for providing the experimental data analyzed in the supplementary material. C.P. is supported by the Italian Institute of Technology (IIT) under the SEED project grant number 259 SIMBEDD Advanced Computational Methods for Biophysics, Drug Design and Energy Research.

Appendix A: Third virial coefficients in the GFVT approach

In this appendix we determine the second and third order virial coefficients predicted by the GFVT expression (13) for the semigrand potential.

To begin with, we determine the low-density expansion of Ω in terms of the virial coefficients. If the pressure has the expansion (22), the canonical free energy can be

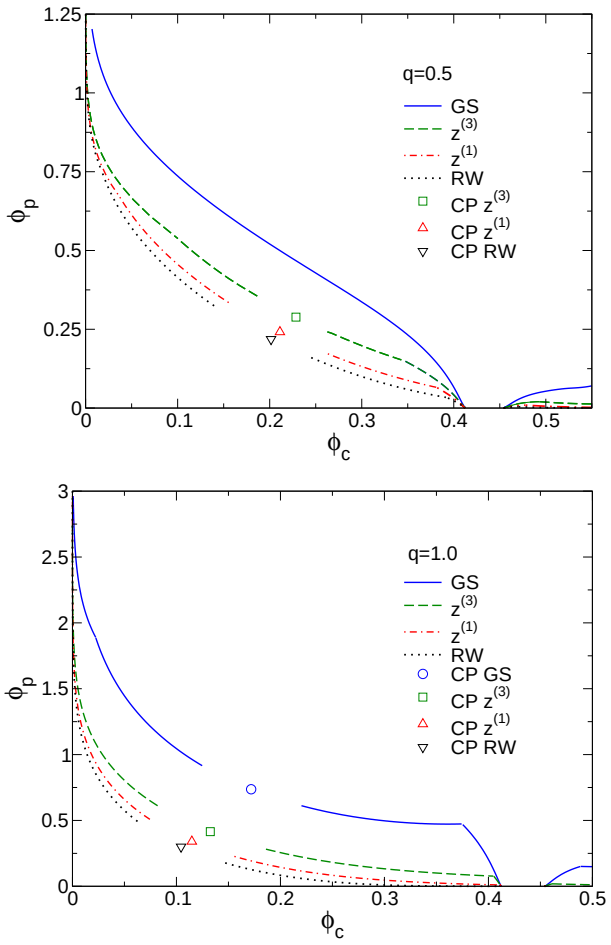

FIG. 11: Phase diagram as a function of ϕ_c and ϕ_p for a system with $s = 1.06$, for several different solvent qualities: good-solvent (GS) conditions, $z = z^{(3)}$, $z = z^{(1)}$, and θ conditions (RW). In the upper panel we report results for $q = 0.5$, in the lower one results for $q = 1$. We also report the critical points (CP). For $q = 0.5$ and good-solvent conditions, no fluid-fluid transition occurs.

expanded as

$$\frac{\beta F_{\rm can}}{V} \approx \rho_c \ln(\rho_c\lambda_c^3) + \rho_p \ln(\rho_p\lambda_p^3) - \rho_c - \rho_p + B_{2,cc}\rho_c^2 + B_{2,pp}\rho_p^2 + B_{2,cp}\rho_c\rho_p + \frac{1}{2}\left(B_{3,ccc}\rho_c^3 + B_{3,ppp}\rho_p^3 + B_{3,ccp}\rho_c^2\rho_p + B_{3,cpp}\rho_c\rho_p^2\right), \quad \text{(A1)}$$

where λ_c and λ_p are the colloid and polymer thermal lengths. The expansion of the chemical potential follows immediately. If $z_p = e^{\beta\mu_p}$, we have

$$z_p/(\lambda_p^3\rho_p) \approx 1 + B_{2,cp}\rho_c + 2B_{2,pp}\rho_p + (B_{2,cp}^2 + B_{3,ccp})\rho_c^2/2 + (4B_{2,pp}^2 + 3B_{3,ppp})\rho_p^2/2 + (2B_{2,cp}B_{2,pp} + B_{3,cpp})\rho_c\rho_p. \quad \text{(A2)}$$

The fugacity z_p can also be expressed in terms of the reservoir polymer density $\rho_p^{(r)}$. Its expansion can be obtained by using Eq. (A2), replacing ρ_p with $\rho_p^{(r)}$, and setting $\rho_c = 0$. These expressions can be used to obtain the expansion of ρ_p in terms of $\rho_p^{(r)}$ and ρ_c. We obtain

$$\rho_p/\rho_p^{(r)} \approx 1 + \rho_c\left[-B_{2,cp} + \frac{1}{2}(B_{2,cp}^2 - B_{3,ccp})\rho_c + (2B_{2,cp}B_{2,pp} - B_{3,cpp})\rho_p^{(r)}\right]. \quad \text{(A3)}$$

We are now in the position to compute

$$\frac{\Omega}{V} = \frac{F_{\rm can}}{V} - \mu_p\rho_p. \quad \text{(A4)}$$

We obtain

$$\frac{\beta\Omega}{V} \approx \frac{\beta F_{\rm coll}(\rho_c)}{V} - \rho_p^{(r)} + \left(B_{2,cp}\rho_c - B_{2,pp}\rho_p^{(r)}\right)\rho_p^{(r)} - B_{3,ppp}(\rho_p^{(r)})^3 + \frac{1}{2}\rho_c\rho_p^{(r)}\left(-B_{2,cp}^2\rho_c + B_{3,ccp}\rho_c + B_{3,cpp}\rho_p^{(r)}\right). \quad \text{(A5)}$$

Let us now consider the GFVT case. The expressions we use for K_p and δ_s have an expansion of the form[52]

$$K_p \approx 1 + 2B_{2,pp}^{(e)}\rho_p + 3B_{3,ppp}^{(e)}, \quad \text{(A6)}$$
$$\delta_s/R_c \approx -1 + C + \frac{1}{3}\frac{\rho_p C}{B_{2,cp}^{(e)}}(B_{3,cpp}^{(e)} - 2B_{2,pp}^{(e)}B_{2,cp}^{(e)}).$$

Here, we set

$$C = (B_{2,cp}^{(e)}/V_c)^{1/3}, \quad \text{(A7)}$$

and the superscript (e) indicates that each quantity is our estimate of the corresponding virial coefficient. If we now expand Eq. (13), we obtain an expansion of the form (A5) with $B_{2,cp} = B_{2,cp}^{(e)}$, $B_{2,pp} = B_{2,pp}^{(e)}$, $B_{3,cpp} = B_{3,cpp}^{(e)}$, $B_{3,ppp} = B_{3,ppp}^{(e)}$. The only nontrivial coefficient is $B_{3,ccp}$, for which we obtain

$$B_{3,ccp} = 8B_{2,cp}^{(e)}V_c + 2V_c^2 - 9\left(B_{2,cp}^{(e)}/V_c\right)^{2/3}V_c^2. \quad \text{(A8)}$$

Eq. (25) follows.

* Electronic address: giuseppe.dadamo@sissa.it
† Electronic address: andrea.pelissetto@roma1.infn.it
‡ Electronic address: carlo.pierleoni@aquila.infn.it

[1] W. C. K. Poon, J. Phys.: Condensed Matter **14**, R859 (2002).
[2] M. Fuchs and K. S. Schweizer, J. Phys.: Condensed Matter **14**, R239 (2002).
[3] R. Tuinier, J. Rieger, and C. G. de Kruif, Adv. Colloid Interface Sci. **103**, 1 (2003).
[4] K. J. Mutch, J. S. van Duijneveldt, and J. Eastoe, Soft Matter **3**, 155 (2007).
[5] G. J. Fleer and R. Tuinier, Adv. Coll. Interface Sci. **143**, 1 (2008).
[6] O. Myakonkaya and J. Eastoe, Adv. Coll. Interface Sci. **149**, 39 (2009).
[7] S. Asakura and F. Oosawa, J. Chem. Phys. **22**, 1255 (1954).
[8] A. Vrij, Pure and Appl. Chem. **48**, 471 (1976).
[9] A. P. Gast, C. K. Hall, and W. B. Russell, J. Colloid Interface Sci. **96**, 251 (1983).
[10] H. N. W. Lekkerkerker, W. C. K. Poon, P. N. Pusey, A. Stroobants, and P. B. Warren, Europhys. Lett. **20**, 559 (1992).
[11] E. J. Meijer and D. Frenkel, J. Chem. Phys. **100**, 6873 (1994).
[12] M. Dijkstra, J. M. Brader, and R. Evans, J. Phys.: Condensed Matter **11**, 10079 (1999).
[13] M. Schmidt, H. Löwen, J. M. Brader, and R. Evans, Phys. Rev. Lett. **85**, 1934 (2000); J. Phys.: Condensed Matter **14**, 9353 (2002).
[14] P. G. Bolhuis, A. A. Louis, and J. P. Hansen, Phys. Rev. Lett. **89**, 128302 (2002).
[15] M. Dijkstra and R. van Roij, Phys. Rev. Lett. **89**, 208303 (2002).
[16] M. Schmidt and A. R. Denton, Phys. Rev. E **65**, 061410 (2002).
[17] T. C. Lee, J. T. Lee, D. R. Pilaski, and M. Robert, Physica A **329**, 411 (2003).
[18] R. L. C. Vink and J. Horbach, J. Phys.: Condens. Matter **16**, S3807 (2004).
[19] R. L. C. Vink and J. Horbach, J. Chem. Phys. **121**, 3253 (2004).
[20] R. L. C. Vink, J. Horbach, and K. Binder, Phys. Rev. E **71**, 011401 (2005).
[21] T. Zykova-Timan, J. Horbach, and K. Binder, J. Chem. Phys. **133**, 014705 (2010).
[22] M. Schmidt, A. R. Denton, and J. M. Brader, J. Chem. Phys. **118**, 1541 (2003).
[23] R. L. C. Vink and M. Schmidt, Phys. Rev. E **71**, 051406 (2005).
[24] J. Zausch, P. Virnau, K. Binder, J. Horbach, R. L. C. Vink, J. Chem. Phys. **130**, 064906 (2009); J. Zausch, J. Horbach, P. Virnau, and K. Binder, J. Phys.: Condens. Matter **22**, 104120 (2010).
[25] M. A. Annunziata and A. Pelissetto, Phys. Rev. E **86**, 041804 (2012).
[26] A. Fortini, P. G. Bolhuis, and M. Dijkstra, J. Chem. Phys. **128**, 024904 (2008).
[27] J. Dzubiella, A. Jusufi, C. N. Likos, C. von Ferber, H. Löwen, J. Stellbrink, J. Allgaier, D. Richter, A. B. Schofield, P. A. Smith, W. C. K. Poon, and P. N. Pusey, Phys. Rev. E **64**, 010401(R) (2001).
[28] J. Dzubiella, C. N. Likos, and H. Löwen, J. Chem. Phys. **116**, 9518 (2002).
[29] R. L. C. Vink, A. Jusufi, J. Dzubiella, and C. N. Likos, Phys. Rev. E **72**, 030401(R) (2005).
[30] D. G. L. Aarts, R. Tuinier, and H. N. W. Lekkerkerker, J. Phys.: Condens. Matt. **14**, 7551 (2002).
[31] G. J. Fleer and R. Tuinier, Phys. Rev. E **76**, 041802 (2007).
[32] R. Tuinier, P. A. Smith, W. C. K. Poon, S. U. Egelhaaf, D. G. A. L. Aarts, H. N. W. Lekkerkerker, and G. J. Fleer, Europhys. Lett. **82**, 68002 (2008).
[33] H. N. W. Lekkerkerker and R. Tuinier, *Colloids and the Depletion Interaction*, Lect. Notes Phys. **833** (Springer, Berlin, 2011).
[34] M. Fuchs and K. S. Schweizer, Europhys. Lett. **51**, 621 (2000).
[35] M. Fuchs and K. S. Schweizer, Phys. Rev. E **64**, 021514 (2001).
[36] S. Ramakrishnan, M. Fuchs, K. S. Schweitzer, and C. F. Zukoski, J. Chem. Phys. **116**, 2201 (2002).
[37] P. Bryk, J. Chem. Phys. **122**, 064902 (2005).
[38] P. Paricaud, S. Varga, and G. Jackson, J. Chem. Phys. **118**, 8525 (2003).
[39] A. Pelissetto and J. P. Hansen, Macromolecules **39**, 9571 (2006).
[40] P. G. Bolhuis, E. J. Meijer, and A. A. Louis, Phys. Rev. Lett. **90**, 068304 (2003).
[41] C.-Y. Chou, T. T. M. Vo, A. Z. Panagiotopoulos, and M. Robert, Physica A **369**, 275 (2006).
[42] N. A. Mahynski, T. Lafitte, and A. Z. Panagiotopoulos, Phys. Rev. E **85**, 051402 (2012).
[43] N. A. Mahynski, B. Irick, and A. Z. Panagiotopoulos, Phys. Rev. E **87**, 022309 (2013).
[44] L. Schäfer, *Excluded Volume Effects in Polymer Solutions* (Springer Verlag, Berlin, 1999).
[45] A. Pelissetto, Macromolecules **39**, 4184 (2006).
[46] R. P. Sear and D. Frenkel, Phys. Rev. E **55**, 1677 (1997).
[47] M. Fasolo and P. Sollich, J. Phys.: Condensed Matter **17**, 797 (2005).
[48] B. H. Zimm, W. H. Stockmayer, and M. Fixman, J. Chem. Phys. **21**, 1716 (1953).
[49] M. Rubinstein and R. H. Colby, *Polymer Physics* (Oxford Univ. Press, Oxford, 2003).
[50] In the supplementary material we collect the relevant formulae for the polymer equation of state and the polymer-colloid depletion thickness that are used throughout the paper, and provide extensive tables of results. We also reanalize experimental data, determining the nonuniversal constants that allow us to map them onto the two-parameter model expressions we use to parametrize the thermal crossover region.
[51] G. D'Adamo, A. Pelissetto, and C. Pierleoni, J. Chem. Phys. **139**, 034901 (2013).
[52] G. D'Adamo, A. Pelissetto, and C. Pierleoni, Mol. Phys. **111**, 3372 (2013).
[53] A. Pelissetto, J. Chem. Phys. **129**, 044901 (2008).
[54] A. Fortini, M. Dijkstra, and R. Tuinier, J. Phys.: Condens. Matter **17**, 7783 (2005).
[55] G. C. Berry, J. Chem. Phys. **44**, 4550 (1966).
[56] T. Norisuye, K. Kawahara, A. Teramoto, and H. Fujita, J. Chem. Phys. **49**, 4330 (1968).

[57] T. Matsumoto, N. Nishioka, and H. Fujita, J. Polymer Sci. Part A-2: Polym. Phys. **10**, 23 (1972).

[58] M. Fukuda, M. Fukutomi, Y. Kato, and T. Hashimoto, J. Polymer Sci.: Polym. Phys. **12**, 871 (1974).

[59] M. Daoud and G. Jannink, J. Phys. (France) **37**, 973 (1976).

[60] P. Flory, *Principles of Polymer Chemistry* (Cornell University Press, Ithaca, NY, 1953).

[61] P. G. de Gennes, Phys. Lett. **38A**, 339 (1972).

[62] N. Clisby, Phys. Rev. Lett. **104**, 55702 (2010).

[63] J. des Cloizeaux and G. Jannink, *Polymers in Solution: Their Modelling and Structure* (Clarendon, Oxford, 1990).

[64] B. Duplantier, J. Phys. (France) **43**, 991 (1982); **47**, 745 (1986); Europhys. Lett. **1**, 491 (1986); J. Chem. Phys. **86**, 4233 (1987); B. Duplantier and G. Jannink, Phys. Rev. Lett. **70**, 3174 (1993).

[65] A. Pelissetto and J.-P. Hansen, J. Chem. Phys. **122**, 134904 (2005).

[66] In experimental work the low-density behavior of the osmotic pressure P of a monodisperse solution is usually written as $P/(RTc) = 1/M + B_{2,\rm expt}c + O(c^2)$, where M is the molar mass of the polymer, c the weight concentration, and T the absolute temperature. Then, $B_2 \equiv M^2 B_{2,\rm expt}/N_A$, where N_A is the Avogadro number. Polydispersity is discussed in the supplementary material (Ref. 50).

[67] S. Caracciolo, B. M. Mognetti, and A. Pelissetto, J. Chem. Phys. **125**, 094903 (2006).

[68] S. Caracciolo, B. M. Mognetti, and A. Pelissetto, J. Chem. Phys. **128**, 065104 (2008).

[69] N. F. Carnahan and K. E. Starling, J. Phys. Chem. **51**, 635 (1969).

[70] D. Frenkel and A. J. C. Ladd, J. Chem. Phys. **81**, 3188 (1984).

[71] H. Reiss, J. Phys. Chem. **96**, 4736 (1992).

[72] Note that the second equation appearing in Aarts *et al.* (Ref. 30) is incorrect. The term $2(\Delta/R_c)^3$ should be replaced by $3(\Delta/R_c)^3$.

[73] G. A. Mansouri, N. F. Carnahan, K. E. Starling, and T. W. Leland, Jr., J. Chem. Phys. **54**, 1523 (1971).

[74] We consider a bidisperse solution of hard spheres of radius R_c and R_p, $R_p/R_c = d$, at volume fractions ϕ_c and ϕ_p and define, see Eq. (21), $\alpha = \lim_{\phi_p\to 0} \phi_p/\phi_p^{(r)}$. In this limit we have $\rho_p^{(r)}\lambda_p^3 = e^{\beta\mu_p}$. Then, if we define the excess chemical potential $\mu_p^{(exc)}$ as $e^{\beta\mu_p} = \rho_p\lambda_p^3 e^{\beta\mu_p^{(exc)}}$, we end up with $\alpha = \lim_{\phi_p\to 0} e^{-\beta\mu_p^{(exc)}}$. Such a quantity can be easily determined from the equation of state of the bidisperse system.

[75] C. Domb and G. S. Joyce, J. Phys. C **5**, 956 (1972).

[76] J. G. Kirkwood and F. P. Buff, J. Chem. Phys. **19**, 774 (1951).

[77] A. Ben-Naim, *Molecular Physics of Solutions* (Ocford Univ. Press, Oxford, 2006).

[78] To extrapolate $A(L,V) = \beta R_c^3/\kappa_T$, we assume $A(L,V) = A_{\rm scal} + bL^{-\nu} + cL^{s\nu}/M^s$, where M is the size of the box (its volume is M^3) and L the chain length. The number s depends on the choice of the finite-volume definition (see Ref. 52, Sec. 5.1), while ν is equal to 0.5876 for good-solvent conditions and $\nu = 1/2$ in the thermal crossover region. Note the peculiar L dependence of the volume correction. It is justified in detail in Ref. 51, Sec. IV.B.

[79] G. J. Fleer, A. M. Skvortsov, and R. Tuinier, Macromol. Theory Simul. **16**, 531 (2007).

[80] A. Hanke, E. Eisenriegler, and S. Dietrich, Phys. Rev. E **59**, 6853 (1999).

[81] R. Maassen, E. Eisenriegler, and A. Bringer, J. Chem. Phys. **115**, 5292 (2001).

[82] P. G. de Gennes, *Scaling Concepts in Polymer Physics* (Cornell University Press, Ithaca, NY, 1979).

[83] Although the leading scaling corrections are equal in continuum and lattice models, the latter show additional scaling corrections. The leading one scales as $L^{-\omega_{nr}\nu}$ with $\omega_{nr} \approx 2$ [M. Campostrini, A. Pelissetto, P. Rossi, and E. Vicari, Phys. Rev. E **57**, 184 (1999)]. Such terms, of order $L^{-1.2}$, are much less relevant than those considered in the extrapolation.

[84] R. Menichetti and A. Pelissetto, J. Chem. Phys. **138**, 124902 (2013).

[85] R. Kniewski and W.-M. Kulicke, Makromol. Chem. **184**, 2173 (1983).

[86] L. J. Fetters, N. Hadjichristidis, J. S. Lindner, and J. W. Mays, J. Phys. Chem. Ref. Data **23**, 619 (1994).

[87] K. Mutch, J. van Duijneveldt, J. Eastoe, I. Grillo, and R. K. Heenan, Langmuir **24**, 3053 (2008).

[88] K. Mutch, J. van Duijneveldt, J. Eastoe, I. Grillo, and R. K. Heenan, Langmuir **25**, 3944 (2009).

[89] K. Mutch, J. van Duijneveldt, J. Eastoe, I. Grillo, and R. K. Heenan, Langmuir **26**, 1630 (2010).

[90] In Ref. 87 it was assumed that $B_{2,\rm expt} = 7.01\cdot 10^{-4}$ mol·cm^3/g^2 (see Ref. 66 for the definition of $B_{2,\rm expt}$) and $R_g = 33$ nm for a sample of polyisoprene of molar weight $M_w = 3.5\cdot 10^5$ g/mol. If these estimates were correct, one would obtain $A_{2,pp} = 2.92$, hence the system would not be under good-solvent conditions. However, a reanalysis of the data of Ref. 91 (see their tables I and IV) gives $B_{2,\rm expt} = 6.37\cdot 10^{-4}$ mol·cm^3/g^2 and $R_g = 30$ nm, hence $A_{2,pp} = 4.80$, which is close to the good-solvent value[67] 5.50.

[91] N. S. Davidson, L. J. Fetters, W. G. Funk, N. Hadjichristidis, and W. W. Graessley, Macromolecules **20**, 2614 (1987).

[92] C. Gögelein and R. Tuinier, Eur. Phys. J. E **27**, 171 (2008).

[93] K. van Gruijthuijsen, R. Tuinier, J. M. Brader, and A. Stradner, Soft Matter **9**, 9977 (2013).

[94] J. A. Barker and D. Henderson, J. Chem. Phys. **47**, 4714 (1967).

Appendix B: Supplementary Material: Analysis of the experimental data

1. Two-parameter approach to thermal crossover

In Section II we discussed the behavior of structural and thermodynamic properties in the thermal crossover region. Here, we wish to compute the nonuniversal constants that allow one to relate theoretical results for Edward's two parameter model (TPM) and experimental data. We will consider the experimental systems studied in Refs. 1–3, which were already analyzed in the TPM framework. However, the TPM expressions used in those analyses are not accurate and, in particular, differ significantly from the correct result close to the good-solvent regime. We have therefore decided to repeat the analyses, matching the experimental results with the very precise TPM predictions for the crossover functions associated with the second virial coefficient and the swelling ratio reported in Refs. 4,5.

Before discussing the experimental results, let us first summarize the basic theoretical ideas, which have already been presented in Sec. II. General renormalization-group arguments[6–8] indicate that, in the thermal crossover region above T_θ, global properties of the polymer solution satisfy a general scaling form:

$$\mathcal{O}(T,L,\rho) = \alpha_1 \mathcal{O}_G(L,\rho) g_{\mathcal{O}}[L^{1/2} f_T(T) (\log L)^{-4/11}, \phi_p]. \tag{B1}$$

Here $\mathcal{O}(T,L,\rho)$ is the value of the observable under consideration as a function of temperature T, the degree of polymerization L, and number density $\rho = N_p/V$, $\mathcal{O}_G(L,\rho) = \mathcal{O}(T_\theta,L,\rho)$ is the value of $\mathcal{O}$ at the θ temperature, $\phi_p = 4\pi\rho R_g^3/3$, where R_g is the radius of gyration of an isolated polymer of degree of polymerization L at temperature T. Chemical details are included in the amplitude α_1 and in the function $f_T(T)$ of the temperature, which vanishes at the θ point: $f_T(T_\theta) = 0$. The function $g_{\mathcal{O}}$, which satisfies $g_{\mathcal{O}}(0,\phi_p) = 1$, is universal, i.e., independent of the microscopic chemical details, and can be identified with the TPM crossover function associated with $\mathcal{O}$.[9] In Eq. (B1) the relevant variable which parametrizes the crossover between θ and good-solvent behavior is the combination $L^{1/2} f_T(T) (\log L)^{-4/11}$. However, the logarithmic dependence on L is hardly measurable in experiments in which L varies by no more than one order of magnitude, hence, as usual in most polymer literature, we will neglect the logarithmic dependence, rewriting Eq. (B1) as

$$\mathcal{O}(T,L,\rho) = \alpha_1 \mathcal{O}_G(L,\rho) g_{\mathcal{O}}[L^{1/2} f_T(T), \phi_p]. \tag{B2}$$

As a second comment, note that Eq. (B1) is strictly valid for $L \to \infty$. Close to the θ point, theory predicts[6–8] corrections that decrease as $1/\ln L$. However, as we discuss below, for the experimental quantities we consider, such corrections are small compared to the typical experimental uncertainties. Therefore, we will neglect these contributions and we will apply Eq. (B2) to the analysis of the experimental systems without introducing any type of logarithmic correction.

To define completely the arguments of the scaling function $g_{\mathcal{O}}$, we must specify the function $f_T(T)$, which represents what is called a *nonlinear scaling field* in the renormalization-group language.[10] It is an analytic function of temperature which vanishes at the θ point. Therefore, it has a regular expansion around $T = T_\theta$ of the form

$$f_T(T) = \alpha_0 (T - T_\theta)[1 + \alpha_1 (T - T_\theta) + \alpha_2 (T - T_\theta)^2 + \ldots]. \tag{B3}$$

The constants α_1, α_2, …, are completely specified by the microscopic details of the model, while α_0 is a normalization system-dependent constant that has to be properly fixed to guarantee the universality of the scaling function $g_{\mathcal{O}}$. Typically, experiments are not so precise to allow us to determine the T dependence of the function $f_T(T)$. Therefore, in the following we shall use two simple expressions that have the correct behavior for $T \to T_\theta$. We will consider

$$f_T^{(1)}(T) = \alpha_0 \frac{T - T_\theta}{T_\theta}, \tag{B4}$$

$$f_T^{(2)}(T) = \alpha_0 \frac{T - T_\theta}{T}. \tag{B5}$$

The first one corresponds to truncating Eq. (B3) at first order (with a simple redefinition of α_0), while the second one is the classical form that can be found in the experimental literature and in popular textbooks of polymer physics (for instance, in Ref. 11). The constant α_0 is fixed by identifying $f_T(T) L^{1/2}$ with the Zimm-Fixman-Stockmayer variable[12] z. In other words, if $g_{\mathcal{O},\mathrm{TPM}}(z,\phi_p)$ is the scaling function associated with $\mathcal{O}$ computed in the TPM, we fix α_0 so that

$$g_{\mathcal{O},\mathrm{TPM}}(z,\phi_p) \approx g_{\mathcal{O}}(z = f_T(T) L^{1/2}, \phi_p). \tag{B6}$$

The use of the two functions $f_T^{(1)}(T)$ and $f_T^{(2)}(T)$ provides slightly different estimates of the constant α_0. Such a difference gives us an indication of the uncertainty on the final result due to fact that we do not have a precise knowledge of the T dependence of $f_T(T)$. Note that, in the TPM framework, α_0 does not depend on the observable $\mathcal{O}$. In other words, if α_0 is fixed by requiring the validity of Eq. (B6) for a given quantity $\mathcal{O}$, Eq. (B6) should also be satisfied by any other quantity.

2. Experimental systems

When comparing with the experimental data, it is more convenient to use the weight-average molar mass

TABLE VI: Polymer solutions considered in the present analysis. For each sample we report the weight-average molar mass M_w, the θ temperature, the zero-density squared radius of gyration $R^2_{g,\theta}$ at the θ point, and the ratio $\ell_k = R_{g,\theta}/M_w^{1/2}$. We also report the polydispersity index M_w/M_n, where M_n is the number-average molar mass.

Polystyrene (PS) in decalin (Ref. 1)[a] $M_w/M_n \lesssim 1.07$				
Sample	$M_w/10^6$ (g·mol^{-1})	$T_\theta(K)$	$R^2_{g,\theta}$ (nm^2)	ℓ_k [nm·(mol/g)$^{1/2}$]
A-30	4.40	288.2	4550	0.0321
A-5	1.56	288.4	1320	0.0291
A-16	1.05	288.2	820	0.0279
A-13	0.186	288.0	158	0.0291
Polychloroprene (PCP) in trans-decalin (Ref. 2) $M_w/M_n \approx 1.1$				
Sample	$M_w/10^6$ (g·mol^{-1})	$T_\theta(K)$	$R^2_{g,\theta}$ (nm^2)	ℓ_k [nm·(mol/g)$^{1/2}$]
f-16B	1.66	274.9	1500	0.0300
f-14B	0.865	274.9	770	0.0298
f-12	0.587	274.9	519	0.0295
Polyisobutilene (PIB) in isoamyl-isovalerate (Ref. 3) $M_w/M_n \approx 1.1$				
Sample	$M_w/10^6$ (g·mol^{-1})	$T_\theta(K)$	$R^2_{g,\theta}$ (nm^2)	ℓ_k [nm·(mol/g)$^{1/2}$]
A-42	4.7	295.1	4500	0.031
A-32	3.1	295.1	3200	0.032
A-73	1.4	≈295.2	1350	0.031
A-54	0.81	≈295.3	730	0.030

[a] Solution of decalin with 61.7% of the cis-isomer. Sample A-5 was also studied in a solution with 51.4% of cis-decalin.

M_w instead of L. Hence, we write z as

$$z = a^{(1)} \frac{T - T_\theta}{T_\theta} M_w^{1/2}, \tag{B7}$$

$$z = a^{(2)} \frac{T - T_\theta}{T} M_w^{1/2}. \tag{B8}$$

Here, we determine the nonuniversal constants $a^{(1)}$ and $a^{(2)}$ for three different polymer solutions that show an extensive thermal crossover close to room temperature: polystyrene (PS) in a mixture of isomers of decalin,[1] polychloroprene (PCP) in trans-decalin,[2] and polyisobutilene (PIB) in isoamyl-isovalerate.[3] We use the experimental results presented in Refs. 1–3. Details are reported in Table VI. The samples are identified by using the same name abbreviations as in the original articles. In all cases the θ temperature is identified as the one at which the second virial coefficient vanishes. In Table VI we also report the ratio ℓ_k defined by

$$\ell_k = R_g(T_\theta, M_w) M_w^{-1/2} \tag{B9}$$

($R_g(T_\theta, M_w)$ is the zero-density readius of gyration), which is expected to be constant at the θ point. Data for PIB and PCP are reasonably constant. Significant variations are instead observed for the PS data. In particular, ℓ_k for the sample with the largest molecular weight is significantly larger than that obtained for the other samples. Berry[1] explained this discrepancy as a polydispersity effect. However, if we assume that $\ell_k \approx 0.0287$ nm·(mol/g)$^{1/2}$ for a monodisperse sample—this is the average of the results for samples A-5,A-16, and A-13—Eq. (B45), which relates R_g^2 for a polydisperse sample with the corresponding monodisperse quantity, gives $M_w/M_n \approx 1.33$. Therefore, the value $\ell_k \approx 0.0321$ nm·(mol/g)$^{1/2}$ can be explained as a polydispersity effect only if the mass distribution is much broader than that observed in fractionation studies of the same samples—they provide $1.01 \lesssim M_w/M_n \lesssim 1.07$. As we shall discuss below, such an interpretation is also inconsistent with the results for the second virial coefficient. More likely, the quoted value for R_g^2 is the result of an incorrect extrapolation to the zero-angle limit (note that in the experiment the angle varies between 18° and 135°), which, as stated by Berry himself, becomes difficult when $R_g^2 \gtrsim 4 \cdot 10^{-11}$ cm^2. For these reasons, we will not use the measured value of R_g^2 for sample A-30. Instead, we will use the scaling formula $R_g^2 = \ell_k^2 M_w$ with $\ell_k \approx 0.0287$ nm·(mol/g)$^{1/2}$. This gives

$$R^2_{g,\theta} = 3620\,\text{nm}^2 \tag{B10}$$

for sample A-30.

To determine the nonuniversal constants, we use two different quantities. First, we consider the swelling ratio

$$\alpha(T, M_w) = \frac{R_g(T, M_w)}{R_g(T_\theta, M_w)}, \tag{B11}$$

where $R_g(T, M_w)$ is the radius of gyration of the polymer in the infinite-dilution limit. For a monodisperse system, such a quantity should approach the TPM prediction[4]

$$\alpha_{TPM}(z) = (1{+}10.9288z{+}35.1869z^2{+}30.4463z^3)^{0.0583867} \tag{B12}$$

for large values of M_w, with a proper choice of the normalization constant. Second, we consider the second virial coefficient $B_{2,\text{expt}}$, which can be determined either by measuring the small density behavior of the osmotic pressure or from scattering experiments in dilute solutions (note that in the presence of polydispersity, these two methods provide different quantities, see Sec. B 5 for the precise definitions). The universal ratio A_2 (to lighten the notation, since we do not consider colloids here, we use A_2 instead of $A_{2,pp}$ as in the text) can be

expressed in terms of $B_{2,\rm expt}$ as

$$A_2(T,M_w) = \frac{M_w^2 B_{2,\rm expt}(T,M_w)}{N_A R_g(T,M_w)^3}, \qquad \text{(B13)}$$

where N_A is Avogadro's number. With a proper identification of the nonuniversal constant, $A_2(T,M_w)$ should approach the TPM expression

$$A_{2,TPM}(z) = 4\pi^{3/2} z (1 + 19.1187 z + 126.783 z^2 + 331.99 z^3 + 268.96 z^4)^{-1/4}. \qquad \text{(B14)}$$

It is important to stress that the TPM expressions (B12) and (B14) refer to a strictly monodisperse sample. In the presence of polydispersity, corrections should be considered. If the swelling ratio is defined in terms of the Z-averaged radius of gyration,[13] which is the quantity obtained in scattering experiments, we have

$$\alpha_Z^2(z) = \alpha(z)^2 C(z), \qquad \text{(B15)}$$

where $C(z)$ is the polydispersity correction, which depends on the polymer mass distribution. The function $C(z)$ is computed in Sec. B 5. If the Schulz distribution is assumed,[13] for systems which satisfy $M_w/M_n \lesssim 1.1$, $C(z)$ represents a small correction, of the order of 2% at most. Therefore, for the swelling ratio, polydispersity effects are negligible, given the uncertainty on the data. On the other hand, polydispersity effect on A_2 are very large, at least in the good-solvent region. For instance, in a system with Schulz parameter $s = 10$ (corresponding to $M_w/M_n = 1.10$), A_2 is 40% smaller than the value obtained for a monodisperse system, see Sec. B 5 and Ref. 14. More precisely, the combination $A_{2,Z}$ which is determined in scattering experiments has a good-solvent value of 4.21 for $s = 10$, while it takes the value[15] 5.50 for a monodisperse solution. The results of Ref. 14 also allow us to exclude that sample A-30 is broadly polydispersed, with $M_w/M_n \approx 1.33$. Indeed, using the Schulz distribution, we would obtain $s \approx 3$. Then, using the results reported in Ref. 14, we would estimate $A_{2,Z} \approx 2.7$ in the good-solvent regime, which is significantly lower than what is obtained experimentally. Indeed, for $T = 363.2$ K and 377.8 K, which are probably close to the good-solvent regime ($T_\theta \approx 288$ K), the experimental results for sample A-30 give $A_2 = 3.94$ and $A_2 = 4.01$, if the measured value of R_g is used. Both values are significantly larger than $A_{2,Z} \approx 2.7$, excluding that polydispersity is the origin of the quite large value for the radius of gyration at the θ point. Note that, if we use instead $R_{g,\theta}^2 = 3620$ nm^2, for $T = 363.2$ K and 377.8 K we obtain $A_2 = 5.34$ and 5.44, which are close to the good-solvent value 5.50 appropriate for monodisperse solutions.[15]

Before computing $a^{(1)}$ and $a^{(2)}$, we verify that the logarithmic scaling corrections related the three-body interactions can be neglected even at the θ point for the experimental quantities we consider. This is of course a necessary requirement to apply TPM results to the data. For this purpose, in Fig. 12 we plot $A_2(T,M_w)$ versus $[\alpha(T,M_w)]^3$. We also report the theoretical TPM curve, obtained by expressing $A_{2,TPM}(z)$ in terms of $[\alpha_{TPM}(z)]^3$. This comparison does not require us to fix the normalization of z, hence there are no free parameters. Within the accuracy of the data, the experimental results fall on top of the theoretical curve. Again, note that it is crucial to correct the results for PS sample A-30. Otherwise, no agreement would be observed for large α^3. Clearly, the logarithmic three-body corrections are not detectable, at least with the experimental resolution of Refs. 1–3. A second clear indication that logarithmic corrections are small for the quantities at hand is the fact that the θ temperature (which is defined as the temperature at which the second virial coefficient vanishes) is essentially independent of M_w. This conclusion is related to the considered quantities and to the precision of the data: for polystyrene in cyclohexane, tricritical effects were observed in Ref. 16 very close to the θ point. Moreover, tricritical corrections are essential to describe the behavior of higher-order virial coefficients. For instance, the experimental results for PS in cyclohexane[17] and for PIB in isoamyl-isovalerate,[18] as well as numerical results for lattice self-avoiding walks,[19] show that the third virial coefficient does not vanish at the θ point and that it increases as T is lowered below T_θ. This behavior cannot be explained by the TPM: in the TPM the third virial coefficient behaves as z^3 close to the θ point (in particular, it is negative below the θ point). Analogously, tricritical effects cannot be neglected in the equation of state in the semidilute regime. Hence, the results presented here apply in general only away from the θ point, in the region in which tricritical effects are negligible. The combination A_2 and the swelling ratio α^2 appear to be exceptions, since the TPM apparently provides a good description of the data even at the θ point.

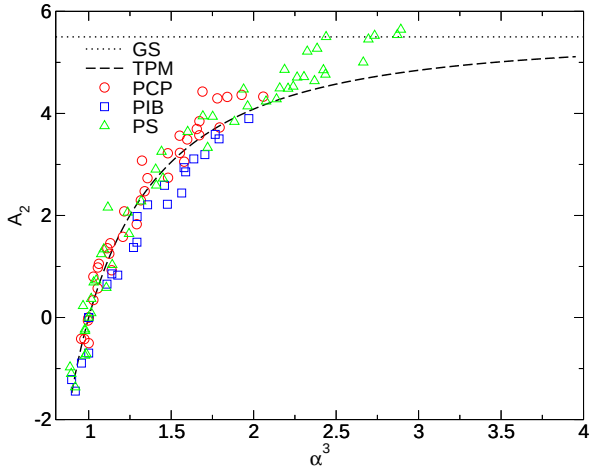

FIG. 12: Combination $A_2(T,M_w)$ versus $\alpha(T,M_w)^3$ for three different experimental systems. The dashed line is the TPM prediction.

TABLE VII: Constants $a^{(1)}$ and $a^{(2)}$ (in units $(\text{mol/g})^{1/2}$), obtained by using different methods: from the analysis of the swelling ratio (α^2), from the analysis of A_2 (A_2), and by using the recursive method of Berry[1] (α^2 B and A_2 B). For the PS estimates obtained by using the recursive method, we also report an error related to the uncertainty with which s_B and s_S are estimated. In the last line we report the results of Ref. 1 for PS, 3 for PIB, and 2 for PCP.

	PS		PIB		PCP	
Method	$a^{(1)}$	$a^{(2)}$	$a^{(1)}$	$a^{(2)}$	$a^{(1)}$	$a^{(2)}$
α^2	0.0047	0.0057	0.0031	0.0035	0.0046	0.0052
A_2	0.0072	0.0084	0.0027	0.0028	0.0056	0.0060
α^2 B	0.0069(4)	0.0066(4)	0.0031	0.0036	0.0049	0.0046
A_2 B	0.0070(5)	0.0074(5)	0.0027	0.0030	0.0051	0.0059
liter.		0.00975		0.003		0.0057

3. Direct determination of the nonuniversal constants

The nonuniversal constants can be determined directly, by requiring the experimental data to match the TPM expression. For instance, if we consider the data for the second virial coefficient, we define

$$R(a^{(i)}) = \sum_a [A_a(T, M_w) - A_{TPM}(z_a)]^2, \qquad \text{(B16)}$$

where the sum is over all experimental data and z_a is computed by using the appropriate function $f_T(T)$, with nonuniversal constant $a^{(i)}$. The function $R(a^{(i)})$ is the usual goodness of the fit, in the absence of any knowledge of the error affecting the experimental data. The value of $a^{(i)}$ is then determined by minimizing R. The results are reported in Table VII (line A_2). The same procedure can be applied to α^2. The corresponding results are reported in Table VII (line α^2).

The results for PIB and PCP show little dependence on the choice of the function $f_T(T)$. This is probably related to the fact that the experimental data belong to a small temperature region ($z \lesssim 1$), so that the linear approximation works well. On the other hand, for PS differences are larger, but in this case data extend up to $z \approx 4$, i.e., one observes the full crossover from θ to good-solvent behavior. The analysis of α^2 and A_2 should in principle provide the same result for the constants $a^{(i)}$. For PIB and PCP, differences are small. They are probably a consequence of experimental errors, polydispersity effects, and scaling corrections. As a final result we quote the average of the estimates obtained by using A_2 and α^2:

$$a^{(1)}(\text{PIB}) = 0.0029\,(\text{mol/g})^{1/2},$$
$$a^{(2)}(\text{PIB}) = 0.0031\,(\text{mol/g})^{1/2}, \qquad \text{(B17)}$$
$$a^{(1)}(\text{PCP}) = 0.0051\,(\text{mol/g})^{1/2},$$
$$a^{(2)}(\text{PCP}) = 0.0056\,(\text{mol/g})^{1/2}. \qquad \text{(B18)}$$

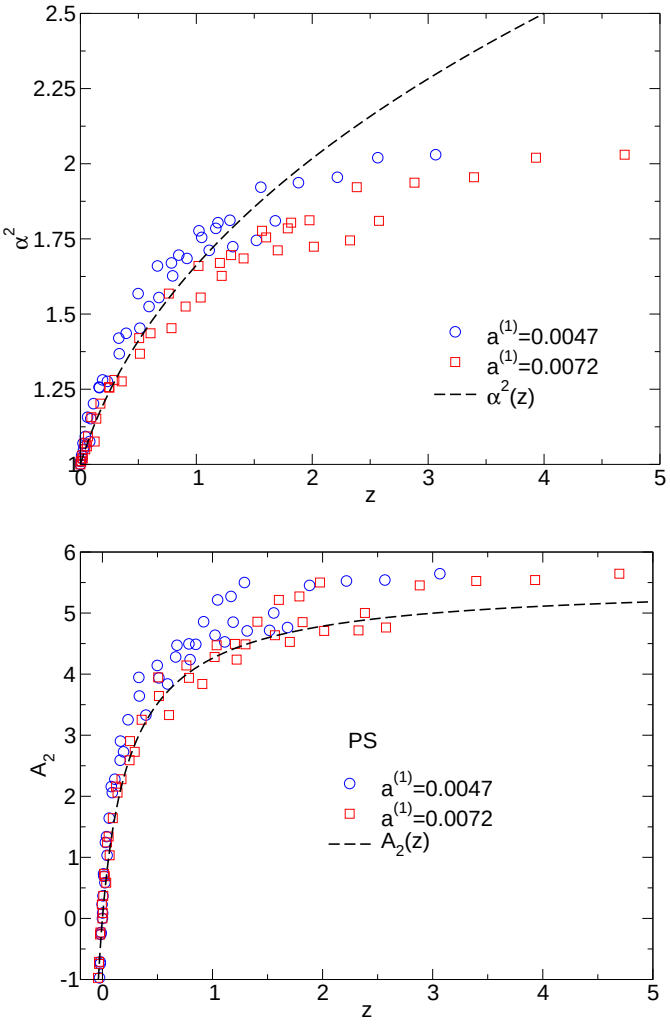

FIG. 13: Comparison of the experimental data for PS (Ref. 1) and the TPM prediction. We define z as in Eq. (B7) and use $a^{(1)} = 0.0047$ $(\text{mol/g})^{1/2}$ and $a^{(1)} = 0.0072$ $(\text{mol/g})^{1/2}$. We report α^2 (top) and A_2 (bottom).

For PS, instead, the results of the two analyses differ quite significantly. One may suspect that the systematic deviations are due the inclusion of sample A-30, for which the radius of gyration was estimated by using the expected scaling at the θ point, see Eq. (B10). To understand the role of data A-30 in the analysis, we have repeated the fitting procedure using only samples A-5 and A-16. From the analysis of α^2 we obtain

$$a^{(1)} = 0.0051\,(\text{mol/g})^{1/2} \qquad a^{(2)} = 0.0061\,(\text{mol/g})^{1/2}, \qquad \text{(B19)}$$

while from the analysis of A_2 we obtain

$$a^{(1)} = 0.0080\,(\text{mol/g})^{1/2} \qquad a^{(2)} = 0.0086\,(\text{mol/g})^{1/2}. \qquad \text{(B20)}$$

Discrepancies are not reduced, allowing us to conclude that the problem does not lie with sample A-30. To un-

derstand better the origin of the observed differences, in Fig. 13 we compare the data for α^2 and A_2 with the TPM predictions. We define z as in Eq. (B7) [similar plots would be obtained by using Eq. (B8)] and use the estimates of $a^{(1)}$ reported in Table VII. For $a^{(1)} = 0.0072$ $(\mathrm{mol/g})^{1/2}$, the estimate obtained from the analysis of A_2, the second-virial coefficient data are quite well described by the TPM curve. The results for α^2 are also quite well described by the TPM curve up to $z \approx 1$. The data for $z \gtrsim 1$ lie instead well below the TPM curve. If we instead use $a^{(1)} = 0.0047$ $(\mathrm{mol/g})^{1/2}$, even the data for α^2 are poorly fitted. Indeed, the best fit is obtained by letting the data close the θ point lie significantly above the TPM curve, while those corresponding to $z \gtrsim 1$ lie somewhat below the TPM curve. Clearly, the value $a^{(1)} = 0.0047$ $(\mathrm{mol/g})^{1/2}$ cannot be trusted. For these reasons, for PS, we only consider the results obtained by using A_2. Hence, we quote

$$a^{(1)}(\mathrm{PS}) = 0.0072\,(\mathrm{mol/g})^{1/2},$$
$$a^{(2)}(\mathrm{PS}) = 0.0084\,(\mathrm{mol/g})^{1/2}. \qquad \text{(B21)}$$

The experimental data are compared with the TPM predictions in Fig. 14. The A_2 data are always reasonably well described by the TPM expression (small deviations are observed for PS close to the good-solvent regime). On the other hand, for the swelling ratio, deviations occur as soon as $z \gtrsim 1$. These deviations are probably due to scaling corrections (polydispersity effects should not be important as we discuss below), which increase as z increases.[15] We can compare our results with those appearing in the literature. While our estimates for PCP and PIB are in good agreement with those of Refs. 2,3, for PS our estimate of $a^{(2)}$ is slightly smaller than the one proposed in Ref. 1. We suspect two possible reasons for this discrepancy. First, in this analysis we only used a subset of the data, samples A-30, A-16, A-5, that have the same percentage of cis-isomer and correspond to polymers with the largest molar mass. Second, in Ref. 1 the crossover function is approximated by its expansion to order z^2, while here we use a precise expression that is valid for all values of z.

Finally, we note that Berry,[1] by using his estimate of the nonuniversal constant, found an excellent agreement between the experimental data for α^3 and the corresponding crossover function of Flory and Fisk (Ref. 20), defined implicitly by

$$\alpha^5(z) - \alpha^3(z) = 0.648 z [1 + 0.969 (1 + 10 z/\alpha^3)^{-2/3}]. \qquad \text{(B22)}$$

Unfortunately, this expression is not consistent with general scaling arguments for large values of z. Indeed, for z large, it predicts $\alpha^5 \propto 0.648 z$, while theory[4] gives $\alpha^5 \propto 2.711 z^{5(2\nu-1)} \approx 2.71 z^{0.87597}$. Moreover, it is significantly different from the accurate expression of Ref. 4. Hence, the agreement appears to be fortuitous, as it is also confirmed by the fact that Flory-Fisk expression does not agree with experiments, once we use the estimates of the nonuniversal constants obtained by using the second-virial coefficient data.

4. Determination of the nonuniversal constants using Berry's method

As we have discussed, for PS a direct estimate of the nonuniversal constants gives results that are somewhat different from those reported in Ref. 1. We wish now to understand the origin of the discrepancy, whether it is due to the expressions of the TPM functions used, or rather to the method used to fix the constants. We thus adopt the method originally proposed by Berry in Ref. 1 and apply it in combination with the precise estimates of the TPM functions of Ref. 4.

To analyze the data for the second virial coefficient, we define a universal ratio that involves only the radius of gyration at the θ point:

$$A_2'(T, M_w) = \frac{M_w^2 B_{2,\mathrm{expt}}(T, M_w)}{N_A R_g(T_\theta, M_w)^3}. \qquad \text{(B23)}$$

It converges to $4\pi^{3/2} z F'(z)$, where

$$F'(z) = \frac{A_2(z)\alpha^3(z)}{4\pi^{3/2} z} \qquad \text{(B24)}$$
$$= \frac{\left(30.4463 z^3 + 35.1869 z^2 + 10.9288 z + 1\right)^{0.17516}}{\left(268.96 z^4 + 331.99 z^3 + 126.783 z^2 + 19.1187 z + 1\right)^{0.25}},$$

where in the last line we have used the accurate expressions for $A_2(z)$ and $\alpha(z)$ of Ref. 4. For z small, $A_2'(z) \approx 4\pi^{3/2} z = 4\pi^{3/2} f_T(T) M_w^{1/2}$. A first estimate of $a^{(1)}$ or $a^{(2)}$ can be obtained by determining the dependence of $B_{2,\mathrm{expt}}(T, M_w)$ close to the θ temperature. We write

$$B_{2,\mathrm{expt}}(T, M_w) = s_B \frac{T - T_\theta}{T_\theta} + \ldots, \qquad \text{(B25)}$$

where the coefficient s_B is independent of M_w in the TPM limit. Then, we obtain

$$a^{(i)} = \frac{s_B}{4\pi^{3/2} N_A \ell_k^3}, \qquad \text{(B26)}$$

where $\ell_k^2 = R_g(T_\theta, M_w)^2/M_w$ (see Table VI). Once a first estimate is available, the procedure is iterated, by setting

$$a^{(i)} = \frac{s_B}{4\pi^{3/2} N_A \ell_k^3 F'(z)}, \qquad \text{(B27)}$$

where, at each step, we use the previous determination of $a^{(i)}$ to determine z in the right-hand side. The procedure converges in a few steps and provides the estimates reported in Table VII. They are slightly different from those obtained in the analysis of the previous section, essentially because here more emphasis is given in reproducing correctly the small-z behavior. In the analysis of

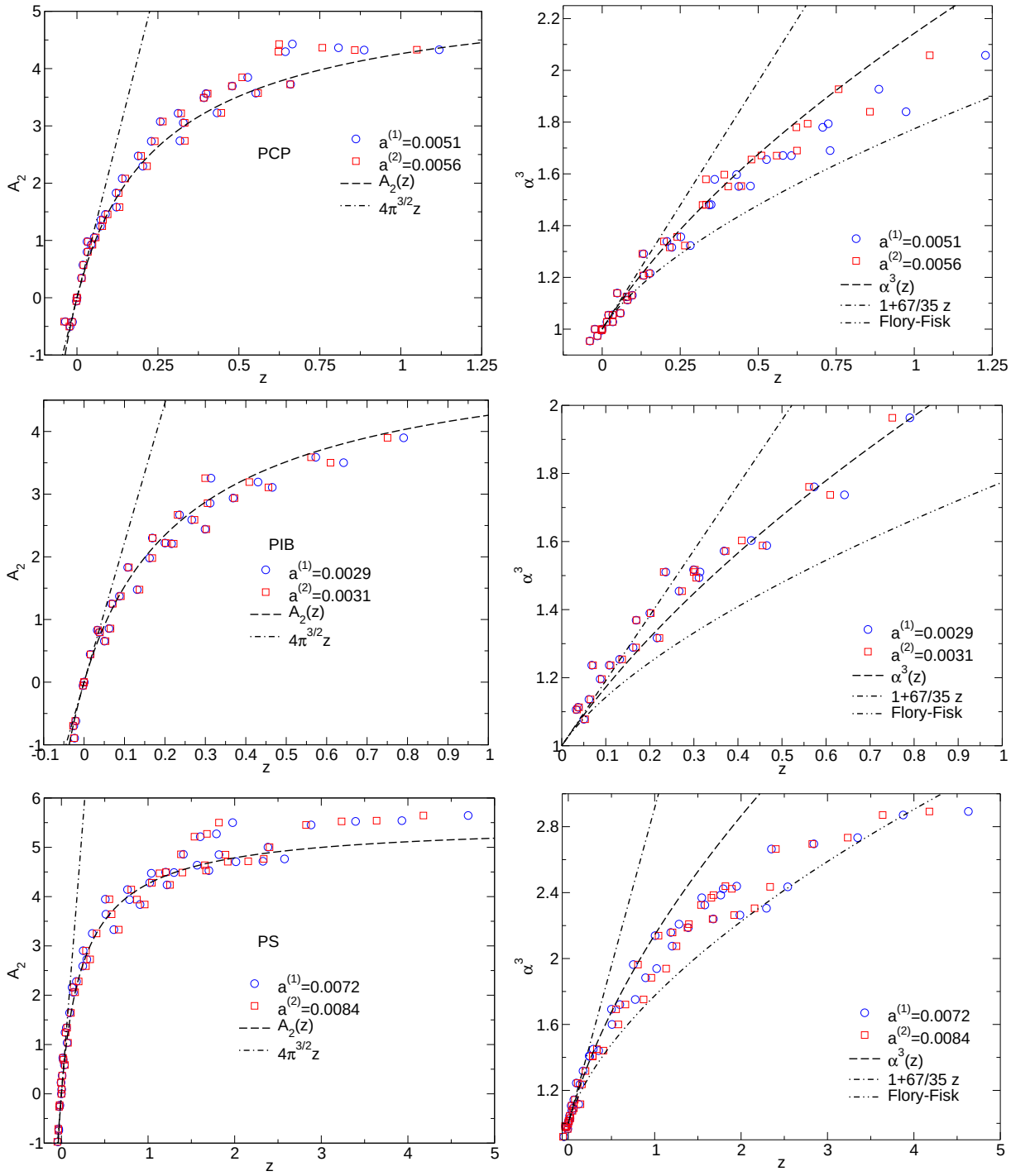

FIG. 14: Comparison of experiments with the TPM predictions. We fix $a^{(1)}$ and $a^{(2)}$ using Eqs. (B18), (B17), and (B21).

Sec. B 3, instead, one aims at obtaining the best approximation in the whole range of values of z considered.

We can use a similar method to analyze the swelling ratio α. We define the ratio

$$S = \frac{R_g^3(T, M_w) - R_g^3(T_\theta, M_w)}{M_w^2}, \tag{B28}$$

which should converge to the TPM expression

$$S \approx \frac{67}{35} \frac{\ell_k^3}{M_w^{1/2}} z G'(z), \tag{B29}$$

where $G'(z)$ is defined as

$$G'(z) = \frac{35}{67}\frac{\alpha^3(z)-1}{z} = \frac{35}{67z} \times \left[\left(1+10.9288z+35.1869z^2+30.4463z^3\right)^{0.17516}-1\right]. \quad \text{(B30)}$$

For $z=0$, we have $G'(0)=1$ (note that $10.9288\times 0.17516 \approx 67/35$). Hence, to compute the nonuniversal constants, we first determine the behavior of S close to the θ point:

$$S(T,M_w) \approx s_S \frac{T-T_\theta}{T_\theta}+\dots \quad \text{(B31)}$$

A first guess for the constants is obtained by setting

$$a^{(1)} = a^{(2)} = \frac{35 s_S}{67\ell_k^3}. \quad \text{(B32)}$$

The procedure is then iterated by setting at each step

$$a^{(i)} = \frac{35 s_S}{67\ell_k^3 G'(z)} \quad \text{(B33)}$$

where z in the right-hand side is computed by using the value of the constants at the previous step. The results are reported in Table VII (line α^2 Berry).

5. Polydispersity effects

In order to compare with experimental results, it is crucial to take into account polydispersity effects. For the ratio A_2, an accurate analysis in the good-solvent regime was presented in Ref. 14. In the polydisperse case, two different virial coefficients can be defined.[13] The weight-averaged $B_{2,\mathrm{expt},w}$ is obtained by measuring the small-density behavior of the (osmotic) pressure:

$$\frac{P}{cRT} = \frac{1}{M_n} + B_{2,\mathrm{expt},w} c + O(c^2), \quad \text{(B34)}$$

where c is the weight concentration. The Z-averaged $B_{2,\mathrm{expt},Z}$ is instead obtained from the the small-concentration behavior of the Rayleigh ratio R_θ measured in scattering experiments:

$$\frac{Kc}{R_\theta} = \frac{1}{M_w} + 2B_{2,\mathrm{expt},Z} c + O(c^2), \quad \text{(B35)}$$

where K is a constant. As for the radius of gyration, scattering experiments provide the Z-averaged square radius of gyration $R^2_{g,Z}$.[13] We can thus define two different ratios corresponding to A_2:

$$A_{2,w} = \frac{B_{2,\mathrm{expt},w} M_w^2}{N_A R^3_{g,Z}}, \quad \text{(B36)}$$

$$A_{2,Z} = \frac{B_{2,\mathrm{expt},Z} M_w^2}{N_A R^3_{g,Z}}, \quad \text{(B37)}$$

where N_A is the Avogadro number. The analysis of the behavior of these two quantities as a function of polydispersity was performed in Ref. 14. The Schulz distribution

$$P(m) = \frac{s}{m_n\Gamma(s)}\left(\frac{sm}{m_n}\right)^{s-1}\exp\left(-\frac{sm}{m_n}\right), \quad \text{(B38)}$$

is usually considered. Here $P(m)$ is the probability of having a polymer of mass m in the solution and m_n is the number-average mass of the polymer (in terms of the number average molar mass $M_n = m_n N_A$), i.e.,

$$m_n = \int_0^\infty m P(m) dm. \quad \text{(B39)}$$

For the Schulz distribution we have

$$\frac{M_w}{M_n} = 1 + 1/s. \quad \text{(B40)}$$

Therefore, since all samples considered in the previous paragraph have $M_w/M_n \lesssim 1.1$, we can conclude that $s \gtrsim 10$. Even though s is quite large so that the distribution is peaked around $m \approx m_n$, the second-virial combinations differ significantly from the monodisperse value $A_{2,\mathrm{mono}} \approx 5.50$.[15] Indeed,[14] for $s=10$ we have $A_{2,w}=3.91$ and $A_{2,Z}=4.21$. Polydispersity effects decrease very slowly, as it can also be seen from the expressions[14]

$$A_{2,w} = 5.50 - 20.5/s, \qquad A_{2,Z} = 5.50 - 16.3/s \quad \text{(B41)}$$

valid for $s \gtrsim 30$. The combinations $A_{2,w}$ and $A_{2,Z}$ are also discussed in Ref. 8 by using perturbative methods. Also field theory predicts large polydispersity corrections, although not as large as determined numerically. At one-loop order, field theory predicts $A_{2,Z} \approx 4.78$ for $s=10$, which, although it differs significantly from the good-solvent value 5.50, is nonetheless larger than the accurate numerical estimate $A_{2,Z}=4.21$.[14]

Let us now consider the effect of polydispersity on the swelling ratio $\alpha(z)$. For a polymer of mass m the zero-density radius of gyration behaves as

$$R_g^2(T,m) = {\ell_k}^2 m f[(mN_A)^{1/2} f_T(T)], \quad \text{(B42)}$$

where $f(z)=\alpha(z)^2$ is the swelling factor computed for a monodisperse system [hence, we can use Eq. (B12)]. It follows that the Z-averaged radius of gyration is given by

$$R^2_{g,Z}(T) = \ell_k^2 \frac{\int_0^\infty m^3 P(m) f[(mN_A)^{1/2} f_T(T)] dm}{\int_0^\infty m^2 P(m) dm}. \quad \text{(B43)}$$

Now, the Schulz distribution can be rewritten as $P(m) = p(m/m_n)/m_n$. Redefining $m = x m_n$ and setting $z =$

$M_w^{1/2} f_T(T)$, we obtain

$$R^2_{g,Z}(T) = \ell_k^2 m_n \frac{\int_0^\infty x^3 p(x) f[(xM_n/M_w)^{1/2} z] dx}{\int_0^\infty x^2 p(x) dx}. \tag{B44}$$

We can use this expression to compare $R^2_{g,Z}(T_\theta)$ for the polydisperse system of weight-averaged mass M_w and $R^2_g(T_\theta, M_w)$ for a monodisperse system of polymers of the same molar mass M_w. For the Schulz distribution we obtain

$$\frac{R^2_{g,Z}(T_\theta)}{R^2_g(T_\theta, M_w)} = \frac{s+2}{s+1} = 2 - \frac{M_n}{M_w}. \tag{B45}$$

For a polydisperse system, we can define an effective swelling ratio as

$$\alpha_Z(z) = \frac{R_{g,Z}(T)}{R_{g,Z}(T_\theta)}, \tag{B46}$$

obtaining

$$\alpha_Z(z)^2 = \frac{\int_0^\infty x^3 p(x) f[(xM_n/M_w)^{1/2} z] dx}{\int_0^\infty x^3 p(x) dx}. \tag{B47}$$

For the Schulz distribution, we obtain explicitly

$$\alpha_Z(z)^2 = \frac{s^2}{(1+s)(2+s)} \int_0^\infty x^3 p(x) f[(sx/(1+s))^{1/2} z] dx. \tag{B48}$$

We define a polydispersity function $C(z,s)$ as

$$\alpha_Z(z)^2 = C(z,s) \alpha(z)^2, \tag{B49}$$

where $\alpha(z)$ is the swelling ratio for a monodisperse system. The function $C(z,s)$ is an increasing function of z which approaches the constant

$$C(z,s) \approx C_\infty(s) = \frac{(1+s)^{1-2\nu} \Gamma(s+2+2\nu)}{\Gamma(s+3)} \tag{B50}$$

for large z. Such a quantity is close to one for any $s \gtrsim 10$. For instance, $C_\infty(s) = 1.108, 1.024$ for $s = 1, 10$, showing that for $s \gtrsim 10$ (i.e., $M_w/M_n \lesssim 1.10$) corrections are at most of 2%. The curve $C(z,s)$ is plotted versus z for a few values of s in Fig. 15.

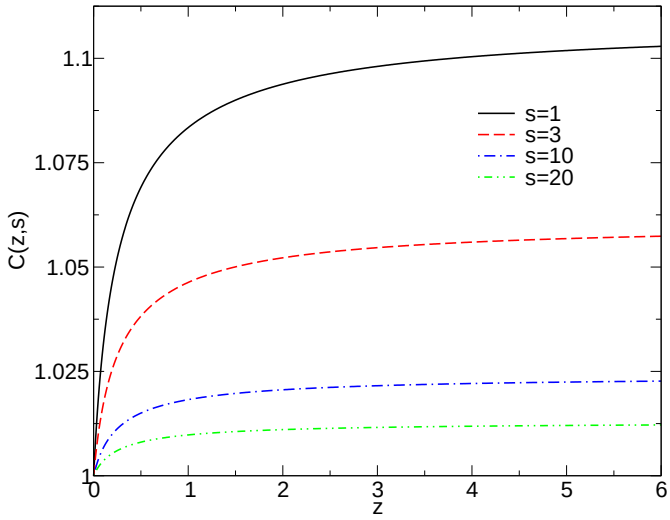

FIG. 15: Polydispersity function $C(z,s)$ for $s = 1, 3, 10, 20$ and $0 \le z \le 6$.

Appendix C: Supplementary material: Polymer properties

1. Depletion thickness

We report here the results for the depletion thickness we used in the paper. They are taken from Ref. 5.

The zero-density depletion thickness $\delta_s(q,0)$ can be expressed in terms of the colloid-polymer second virial combination $A_{2,cp}$, as[5]

$$\frac{\delta_s(q,0)}{R_c} = -1 + \left(\frac{3q^3 A_{2,cp}}{4\pi}\right)^{1/3}. \tag{C1}$$

The quantity $A_{2,cp}$ has been accurately determined by Monte Carlo simulations. The results can be parametrized as

$$A_{2,cp} = \frac{4\pi}{3q^3}\left[\frac{1 + a_1 q + a_2 q^2 + a_3 q^3}{1 + a_4 q}\right]^{1/(2\nu)}, \tag{C2}$$

where $\nu = 0.5876$ for the good-solvent case and $\nu = 1/2$ for $z = z^{(1)}$ and $z^{(3)}$. The coefficients a_i are reported in Table VIII.

TABLE VIII: Coefficients parametrizing $A_{2,cp}$: The interpolation is accurate in the range $0 \le q \le q_{\max}$.

	z	a_1	a_2	a_3	a_4	β	$q_{\max}$
$A_{2,cp}$	∞	4.1329	5.4906	2.12578	0.3942		50
	z_3	3.4774	3.37453	0.39752	0.15763		3
	z_1	3.4378	3.18934	0.20253	0.071526		30

For $q \lesssim 2$, which are the values of q investigated in Ref. 5, the ratio $\delta_s(q,\phi_p)/\delta_s(q,0)$ shows a tiny dependence on q. The results for $q = 0$ (good-solvent case only) and $q = 0.5, 1, 2$ can be parametrized as

$$\frac{\delta_s(q,\phi_p)}{\delta_s(q,0)} = \left(1 + \sum_{k=1}^n a_k \phi_p^k\right)^{-\eta/n}. \tag{C3}$$

The corresponding coefficients are reported in Table IX.

TABLE IX: Coefficients parametrizing the depletion-thickness interpolations (C3) as function of density. The parametrizations should hold for $\phi_p \le \phi_{\max}$.

z	q	n	a_1	a_2	a_3	η	$\phi_{\max}$
∞	0	3	3.9467	4.3305	5.8889	0.770	4
	0.5	3	4.0909	6.8272	2.6728	0.770	4
	1.0	3	4.0987	4.4818	4.92968	0.770	4
	2.0	3	4.0753	6.12348	1.92624	0.770	4
$z^{(3)}$	0.5	2	1.8641	1.0753	0	0.5579	2
	1.0	2	1.8747	1.0279	0	0.5579	4
	2.0	2	2.0279	1.16915	0	0.5128	4
$z^{(1)}$	0.5/1.0/2.0	3	1.7682	1.8151	0.6591	0.2845	4

TABLE X: Coefficients for the interpolations of the compressibility factor $Z = \beta P/\rho_p$ obtained from the full-monomer results for K.

z	a_1	a_2	a_3	a_4	b
$z^{(1)}$	0.455489	0.057089	−0.00117019	−0.0184279	—
$z^{(3)}$	2.69479	3.07853	1.79532	0.614611	1.04964
∞	2.50342	2.54540	1.02975	0.500318	0.6555

For values of q that differ from those considered in Ref. 5, we use a linear interpolation if possible. For $2 \le q \le 3$, we simply set $\delta_s(q,\phi_p)/\delta_s(q,0) = \delta_s(2,\phi_p)/\delta_s(2,0)$ and analogously, for $q \le 0.5$ and $z \ne \infty$, we set $\delta_s(q,\phi_p)/\delta_s(q,0) = \delta_s(0.5,\phi_p)/\delta_s(0.5,0)$.

In the paper we also consider the expression for the depletion thickness proposed in Refs. 21,22 for colloids in good-solvent polymers:

$$\delta_s/R_c = 0.865 q^{0.88}(1 + 3.95\phi_p^{1.54})^{-0.44}. \qquad \text{(C4)}$$

As already discussed in Ref. 5, this expression is in agreement with Monte Carlo full-monomer results and with renormalization-group predictions only for $0.2 \lesssim q \lesssim 4$.

2. Full-monomer equation of state

One of the quantities needed in the GFVT calculation is the pressure derivative $K(\phi_p)$ for the polymer system in the absence of colloids. Such a quantity has been derived from the explicit expressions for the compressibility factor $Z = \beta P/\rho$ reported in Ref. 23 (good-solvent case) and in Ref. 24 ($z = z^{(1)}$ and $z = z^{(3)}$).
For $z = z^{(1)}$ we parametrize the compressibility factor as

$$Z(z^{(1)},\phi_p) = \frac{\sqrt{1 + a_1\phi_p + a_2\phi_p^2 + a_3\phi_p^3}}{\sqrt{1 + a_4\phi_p}}, \qquad \text{(C5)}$$

which behaves linearly for large ϕ_p. For $z = z^{(3)}$ and $\phi_p \lesssim 30$, we use

$$Z(z^{(3)},\phi_p) = (1 + a_1\phi_p + a_2\phi_p^2 + a_3\phi_p^3 + a_4\phi_p^4)^{b/4}, \qquad \text{(C6)}$$

For the good-solvent case we use the parametrization

$$Z(z=\infty,\phi_p) = \frac{(1 + a_1\phi_p + a_2\phi_p^2 + a_3\phi_p^3)^b}{(1 + a_4\phi_p)^b}. \qquad \text{(C7)}$$

The coefficients are reported in Table X. These parametrizations are found to be accurate with deviations of less than 1%.

In the paper we will also consider the expression for K proposed in Refs. 21,22 for polymers under good-solvent conditions:

$$K(\phi_p) = 1 + 3.73\phi_p^{1.31}. \qquad \text{(C8)}$$

This expression agrees (small deviations only occur in the dilute regime) with numerical simulations[23] and field-theory predictions.[8]

Appendix D: Supplementary matherial: GFVT results

We report here some numerical GFVT results. In Tables XI, XII, and XIII, we give the critical-point position for different values of q (up to $q = 3$) and for the three different types of solvent quality we consider in the paper. In Table XIV we report the analogous quantity for non-interacting polymers. We report the polymer and colloid volume fractions at the critical point, the corresponding reservoir polymer volume fraction, the reduced critical pressure $\widetilde{P} = \beta P V_c$, and the excess chemical potentials.

In Tables XV, XVI, XVII, and XVIII we report the triple-point position. We give the reduced triple-point pressure $\widetilde{P} = \beta P V_c$, and the volume fractions of the three coexisting phases.

TABLE XI: Critical-point position, critical pressure ($\widetilde{P} = \beta P V_c$), and excess chemical potentials for the good-solvent case.

z	q	$\phi^{(r)}_{p,\mathrm{crit}}$	$\phi_{c,\mathrm{crit}}$	$\phi_{p,\mathrm{crit}}$	$\tilde{P}_{\mathrm{crit}}$	$\beta\mu^{(exc)}_{c,\mathrm{crit}}$	$\beta\mu^{(exc)}_{p,\mathrm{crit}}$
∞	0.45	0.496	0.299	0.196	9.85	22.8	2.42
	0.50	0.533	0.280	0.217	8.02	19.6	2.51
	0.55	0.570	0.263	0.239	6.70	17.1	2.61
	0.60	0.608	0.249	0.261	5.72	15.3	2.72
	0.65	0.647	0.236	0.284	4.97	13.8	2.83
	0.70	0.687	0.225	0.308	4.39	12.7	2.95
	0.75	0.728	0.215	0.332	3.92	11.7	3.08
	0.80	0.770	0.207	0.357	3.55	10.9	3.22
	0.85	0.813	0.198	0.386	3.25	10.3	3.36
	0.90	0.858	0.190	0.414	3.00	9.71	3.50
	0.95	0.903	0.184	0.442	2.79	9.24	3.66
	1.00	0.951	0.178	0.474	2.61	8.85	3.83
	1.05	0.996	0.172	0.502	2.45	8.47	3.99
	1.10	1.042	0.167	0.533	2.31	8.15	4.15
	1.15	1.088	0.162	0.563	2.19	7.86	4.33
	1.20	1.136	0.157	0.595	2.08	7.61	4.50
	1.25	1.184	0.153	0.627	1.99	7.38	4.69
	1.30	1.233	0.150	0.660	1.90	7.18	4.88
	1.35	1.283	0.146	0.694	1.83	7.01	5.08
	1.40	1.334	0.143	0.728	1.77	6.85	5.28
	1.45	1.386	0.139	0.765	1.71	6.70	5.49
	1.50	1.438	0.136	0.801	1.65	6.57	5.70
	1.55	1.492	0.134	0.837	1.61	6.46	5.92
	1.60	1.546	0.131	0.875	1.57	6.35	6.15
	1.65	1.601	0.129	0.914	1.53	6.26	6.38
	1.70	1.657	0.126	0.954	1.49	6.17	6.62
	1.75	1.713	0.124	0.994	1.46	6.09	6.87
	1.80	1.771	0.122	1.034	1.43	6.02	7.12
	1.85	1.829	0.120	1.077	1.41	5.96	7.38
	1.90	1.888	0.119	1.118	1.38	5.90	7.65
	1.95	1.948	0.117	1.162	1.36	5.85	7.92
	2.00	2.009	0.115	1.205	1.34	5.80	8.20
	2.05	2.082	0.114	1.259	1.34	5.79	8.53
	2.10	2.156	0.113	1.314	1.34	5.79	8.88
	2.15	2.232	0.111	1.370	1.34	5.79	9.24
	2.20	2.311	0.110	1.429	1.34	5.80	9.61
	2.25	2.391	0.110	1.488	1.34	5.82	10.0
	2.30	2.475	0.109	1.549	1.35	5.83	10.4
	2.35	2.560	0.108	1.613	1.36	5.86	10.8
	2.40	2.648	0.107	1.679	1.37	5.89	11.3
	2.45	2.738	0.107	1.748	1.38	5.92	11.7
	2.50	2.831	0.106	1.816	1.39	5.96	12.2
	2.55	2.926	0.106	1.887	1.40	6.00	12.7
	2.60	3.025	0.105	1.963	1.42	6.04	13.2
	2.65	3.126	0.105	2.036	1.44	6.09	13.7
	2.70	3.229	0.105	2.114	1.45	6.14	14.3
	2.75	3.336	0.104	2.196	1.48	6.20	14.9
	2.80	3.446	0.104	2.276	1.50	6.26	15.5
	2.85	3.558	0.104	2.359	1.52	6.32	16.1
	2.90	3.674	0.104	2.449	1.55	6.39	16.7
	2.95	3.793	0.104	2.538	1.57	6.46	17.4
	3.00	3.915	0.104	2.630	1.60	6.54	18.1

TABLE XII: Critical-point position, critical pressure $\widetilde{P} = \beta P V_c$, and excess chemical potentials for $z = z^{(3)}$.

z	q	$\phi^{(r)}_{p,\mathrm{crit}}$	$\phi_{c,\mathrm{crit}}$	$\phi_{p,\mathrm{crit}}$	$\tilde{P}_{\mathrm{crit}}$	$\beta\mu^{(exc)}_{c,\mathrm{crit}}$	$\beta\mu^{(exc)}_{p,\mathrm{crit}}$
$z^{(3)}$	0.40	0.391	0.288	0.141	8.07	19.7	1.59
	0.45	0.420	0.265	0.155	6.21	16.3	1.61
	0.50	0.449	0.246	0.170	4.94	13.8	1.64
	0.55	0.479	0.228	0.185	4.04	12.0	1.66
	0.60	0.509	0.213	0.200	3.37	10.6	1.69
	0.65	0.539	0.200	0.216	2.86	9.46	1.72
	0.70	0.569	0.188	0.231	2.47	8.56	1.75
	0.75	0.600	0.178	0.247	2.15	7.82	1.79
	0.80	0.631	0.169	0.262	1.90	7.21	1.82
	0.85	0.662	0.160	0.278	1.70	6.69	1.86
	0.90	0.694	0.153	0.295	1.53	6.25	1.90
	0.95	0.726	0.146	0.311	1.38	5.87	1.94
	1.00	0.758	0.139	0.329	1.26	5.54	1.98
	1.05	0.791	0.133	0.345	1.16	5.25	2.03
	1.10	0.824	0.128	0.362	1.07	4.99	2.08
	1.15	0.857	0.123	0.381	0.989	4.77	2.12
	1.20	0.890	0.119	0.398	0.921	4.56	2.17
	1.25	0.924	0.114	0.417	0.861	4.39	2.21
	1.30	0.958	0.110	0.435	0.807	4.22	2.26
	1.35	0.992	0.106	0.453	0.759	4.07	2.31
	1.40	1.026	0.103	0.473	0.717	3.94	2.36
	1.45	1.061	0.100	0.491	0.678	3.81	2.41
	1.50	1.096	0.096	0.511	0.645	3.70	2.46
	1.55	1.131	0.093	0.531	0.612	3.60	2.51
	1.60	1.166	0.091	0.550	0.583	3.50	2.57
	1.65	1.202	0.088	0.570	0.557	3.41	2.62
	1.70	1.237	0.086	0.591	0.533	3.33	2.67
	1.75	1.273	0.083	0.611	0.511	3.26	2.73
	1.80	1.309	0.081	0.632	0.491	3.19	2.78
	1.85	1.345	0.079	0.654	0.472	3.12	2.84
	1.90	1.382	0.077	0.674	0.455	3.06	2.90
	1.95	1.418	0.075	0.695	0.438	3.00	2.95
	2.00	1.455	0.073	0.716	0.423	2.95	3.01
	2.05	1.493	0.071	0.741	0.410	2.90	3.07
	2.10	1.532	0.070	0.763	0.397	2.86	3.13
	2.15	1.571	0.069	0.787	0.386	2.82	3.20
	2.20	1.611	0.067	0.811	0.375	2.78	3.26
	2.25	1.651	0.066	0.832	0.365	2.74	3.32
	2.30	1.691	0.064	0.858	0.355	2.70	3.39
	2.35	1.731	0.063	0.882	0.346	2.67	3.45
	2.40	1.772	0.062	0.910	0.338	2.64	3.52
	2.45	1.813	0.061	0.934	0.330	2.61	3.58
	2.50	1.854	0.060	0.960	0.322	2.59	3.65
	2.55	1.896	0.059	0.987	0.315	2.56	3.72
	2.60	1.938	0.057	1.014	0.308	2.54	3.79
	2.65	1.980	0.057	1.038	0.302	2.51	3.86
	2.70	2.023	0.056	1.067	0.296	2.49	3.93
	2.75	2.066	0.055	1.092	0.290	2.47	4.00
	2.80	2.109	0.054	1.123	0.285	2.45	4.07
	2.85	2.153	0.053	1.149	0.280	2.43	4.15
	2.90	2.197	0.052	1.176	0.275	2.41	4.22
	2.95	2.241	0.051	1.204	0.270	2.40	4.30
	3.00	2.286	0.051	1.232	0.266	2.38	4.37

TABLE XIII: Critical-point position, critical pressure ($\widetilde{P} = \beta P V_c$, and excess chemical potentials for $z = z^{(1)}$.

z	q	$\phi^{(r)}_{p,\mathrm{crit}}$	$\phi_{c,\mathrm{crit}}$	$\phi_{p,\mathrm{crit}}$	$\tilde{P}_{\mathrm{crit}}$	$\beta\mu^{(exc)}_{c,\mathrm{crit}}$	$\beta\mu^{(exc)}_{p,\mathrm{crit}}$
$z^{(1)}$	0.35	0.348	0.300	0.116	8.99	21.4	1.26
	0.40	0.376	0.271	0.130	6.57	17.0	1.24
	0.45	0.405	0.248	0.143	5.01	14.0	1.23
	0.50	0.433	0.228	0.155	3.95	11.8	1.23
	0.55	0.462	0.210	0.168	3.19	10.2	1.23
	0.60	0.491	0.195	0.181	2.64	8.96	1.23
	0.65	0.520	0.183	0.193	2.22	7.98	1.24
	0.70	0.550	0.170	0.207	1.89	7.19	1.24
	0.75	0.579	0.161	0.218	1.64	6.54	1.25
	0.80	0.610	0.151	0.232	1.43	6.00	1.26
	0.85	0.640	0.143	0.245	1.26	5.55	1.27
	0.90	0.671	0.135	0.259	1.13	5.16	1.27
	0.95	0.703	0.127	0.274	1.01	4.83	1.28
	1.00	0.734	0.121	0.287	0.913	4.54	1.29
	1.05	0.766	0.115	0.301	0.830	4.28	1.30
	1.10	0.799	0.110	0.316	0.758	4.06	1.31
	1.15	0.831	0.105	0.323	0.696	3.86	1.32
	1.20	0.864	0.100	0.346	0.642	3.69	1.33
	1.25	0.897	0.096	0.360	0.595	3.53	1.34
	1.30	0.931	0.092	0.374	0.553	3.38	1.36
	1.35	0.965	0.088	0.391	0.516	3.25	1.37
	1.40	0.999	0.085	0.406	0.483	3.14	1.38
	1.45	1.033	0.081	0.422	0.453	3.03	1.39
	1.50	1.068	0.079	0.438	0.426	2.93	1.40
	1.55	1.103	0.076	0.455	0.402	2.84	1.42
	1.60	1.138	0.073	0.471	0.380	2.76	1.43
	1.65	1.174	0.070	0.488	0.360	2.68	1.44
	1.70	1.210	0.068	0.504	0.342	2.61	1.46
	1.75	1.246	0.066	0.521	0.325	2.54	1.47
	1.80	1.282	0.064	0.539	0.310	2.49	1.48
	1.85	1.319	0.062	0.555	0.296	2.43	1.50
	1.90	1.355	0.060	0.572	0.283	2.37	1.51
	1.95	1.392	0.058	0.594	0.271	2.33	1.52
	2.00	1.430	0.056	0.610	0.259	2.28	1.54
	2.05	1.467	0.054	0.631	0.249	2.24	1.55
	2.10	1.505	0.053	0.649	0.239	2.20	1.57
	2.15	1.542	0.051	0.668	0.230	2.16	1.58
	2.20	1.581	0.050	0.683	0.222	2.12	1.60
	2.25	1.619	0.049	0.704	0.214	2.09	1.61
	2.30	1.657	0.047	0.726	0.207	2.06	1.63
	2.35	1.696	0.046	0.744	0.200	2.03	1.64
	2.40	1.735	0.045	0.762	0.193	2.00	1.66
	2.45	1.774	0.044	0.782	0.187	1.97	1.68
	2.50	1.813	0.043	0.803	0.181	1.95	1.69
	2.55	1.852	0.042	0.824	0.175	1.92	1.71
	2.60	1.892	0.041	0.840	0.170	1.90	1.73
	2.65	1.931	0.040	0.864	0.165	1.88	1.74
	2.70	1.971	0.039	0.881	0.161	1.85	1.76
	2.75	2.011	0.038	0.906	0.156	1.84	1.77
	2.80	2.052	0.037	0.925	0.152	1.82	1.79
	2.85	2.092	0.037	0.945	0.148	1.80	1.81
	2.90	2.132	0.036	0.965	0.144	1.78	1.83
	2.95	2.173	0.035	0.986	0.141	1.76	1.84
	3.00	2.214	0.034	1.008	0.137	1.75	1.86

TABLE XIV: Critical-point position, critical pressure ($\widetilde{P} = \beta P V_c$), and excess chemical potentials for $z = 0$.

z	q	$\phi^{(r)}_{p,\mathrm{crit}}$	$\phi_{c,\mathrm{crit}}$	$\phi_{p,\mathrm{crit}}$	$\tilde{P}_{\mathrm{crit}}$	$\beta\mu^{(exc)}_{c,\mathrm{crit}}$	$\beta\mu^{(exc)}_{p,\mathrm{crit}}$
0	0.35	0.343	0.290	0.113	8.19	20.0	0
	0.40	0.371	0.264	0.123	5.95	15.8	0
	0.45	0.399	0.239	0.136	4.51	13.0	0
	0.50	0.427	0.219	0.147	3.53	10.9	0
	0.55	0.455	0.201	0.159	2.84	9.42	0
	0.60	0.484	0.187	0.170	2.33	8.25	0
	0.65	0.513	0.174	0.180	1.95	7.33	0
	0.70	0.542	0.161	0.192	1.65	6.59	0
	0.75	0.572	0.150	0.204	1.42	5.98	0
	0.80	0.602	0.141	0.214	1.24	5.47	0
	0.85	0.633	0.133	0.226	1.09	5.05	0
	0.90	0.663	0.125	0.237	0.96	4.68	0
	0.95	0.695	0.118	0.249	0.86	4.37	0
	1.00	0.726	0.111	0.261	0.770	4.10	0
	1.05	0.758	0.106	0.271	0.696	3.86	0
	1.10	0.790	0.100	0.283	0.632	3.65	0
	1.15	0.823	0.095	0.295	0.577	3.46	0
	1.20	0.855	0.090	0.308	0.529	3.30	0
	1.25	0.889	0.086	0.319	0.486	3.15	0
	1.30	0.922	0.082	0.331	0.449	3.01	0
	1.35	0.956	0.078	0.343	0.417	2.89	0
	1.40	0.990	0.075	0.355	0.387	2.79	0
	1.45	1.024	0.071	0.367	0.361	2.68	0
	1.50	1.059	0.069	0.379	0.338	2.59	0
	1.55	1.094	0.066	0.392	0.316	2.50	0
	1.60	1.129	0.063	0.404	0.297	2.42	0
	1.65	1.164	0.060	0.417	0.280	2.35	0
	1.70	1.200	0.058	0.432	0.264	2.29	0
	1.75	1.235	0.056	0.445	0.249	2.23	0
	1.80	1.271	0.054	0.455	0.236	2.17	0
	1.85	1.308	0.052	0.471	0.224	2.12	0
	1.90	1.344	0.050	0.483	0.212	2.07	0
	1.95	1.381	0.048	0.498	0.202	2.03	0
	2.00	1.418	0.046	0.508	0.192	1.98	0
	2.05	1.455	0.045	0.520	0.183	1.94	0
	2.10	1.492	0.043	0.538	0.175	1.91	0
	2.15	1.530	0.041	0.552	0.167	1.87	0
	2.20	1.567	0.040	0.561	0.160	1.83	0
	2.25	1.605	0.039	0.578	0.153	1.80	0
	2.30	1.643	0.038	0.589	0.147	1.77	0
	2.35	1.681	0.037	0.601	0.141	1.74	0
	2.40	1.720	0.035	0.622	0.136	1.72	0
	2.45	1.758	0.034	0.629	0.130	1.69	0
	2.50	1.797	0.033	0.644	0.125	1.67	0
	2.55	1.836	0.032	0.661	0.121	1.65	0
	2.60	1.875	0.031	0.679	0.116	1.63	0
	2.65	1.914	0.030	0.689	0.112	1.61	0
	2.70	1.953	0.030	0.700	0.108	1.58	0
	2.75	1.992	0.029	0.721	0.105	1.57	0
	2.80	2.032	0.028	0.734	0.101	1.55	0
	2.85	2.071	0.027	0.748	0.098	1.54	0
	2.90	2.111	0.026	0.763	0.095	1.52	0
	2.95	2.156	0.024	0.831	0.092	1.57	0
	3.00	2.202	0.023	0.866	0.089	1.58	0

TABLE XV: Triple points: (ϕ_{cg}, ϕ_{pg}), (ϕ_{cl}, ϕ_{pl}) (ϕ_{cs}, ϕ_{ps}) are the volume fractions of the three coexisting phases, $\widetilde{P}_{tp} = \beta P_{tp} V_c$ is the corresponding reduced pressure. Good-solvent case.

z	q	$\phi_{tp}^{(r)}$	ϕ_{cg}	ϕ_{pg}	ϕ_{cl}	ϕ_{pl}	ϕ_{cs}	ϕ_{ps}	$\widetilde{P}_{tp}$
0.5	0.607	0.107	0.468	0.436	0.100	0.578	0.017	9.70	
0.6	0.797	0.043	0.719	0.458	0.096	0.568	0.021	8.69	
0.7	1.01	0.021	0.961	0.466	0.104	0.563	0.026	8.22	
0.8	1.24	0.012	1.21	0.470	0.120	0.561	0.031	8.01	
0.9	1.49	0.0076	1.46	0.471	0.141	0.560	0.038	7.93	
1.0	1.75	0.0053	1.73	0.472	0.167	0.559	0.046	7.92	
1.1	2.02	0.0040	2.00	0.473	0.191	0.559	0.054	7.89	
1.2	2.29	0.0033	2.28	0.473	0.217	0.559	0.062	7.88	
1.3	2.58	0.0028	2.56	0.473	0.246	0.559	0.071	7.89	
1.4	2.89	0.0024	2.86	0.473	0.276	0.559	0.080	7.91	
1.5	3.16	0.0021	3.15	0.473	0.309	0.559	0.090	7.93	
1.6	3.47	0.0019	3.46	0.473	0.343	0.559	0.100	7.95	
1.7	3.78	0.0018	3.77	0.473	0.379	0.559	0.111	7.99	
1.8	4.10	0.0017	4.09	0.473	0.417	0.559	0.123	8.02	
1.9	4.42	0.0016	4.42	0.472	0.456	0.560	0.135	8.05	
2.0	4.75	0.0015	4.75	0.472	0.498	0.560	0.148	8.08	

TABLE XVI: Triple points: (ϕ_{cg}, ϕ_{pg}), (ϕ_{cl}, ϕ_{pl}) (ϕ_{cs}, ϕ_{ps}) are the volume fractions of the three coexisting phases, $\widetilde{P}_{tp}$ is the corresponding reduced pressure. Results for $z = z^{(3)}$.

z	q	$\phi_{tp}^{(r)}$	ϕ_{cg}	ϕ_{pg}	ϕ_{cl}	ϕ_{pl}	ϕ_{cs}	ϕ_{ps}	$\widetilde{P}_{tp}$
0.4	0.439	0.114	0.323	0.437	0.056	0.576	0.0070	9.21	
0.5	0.632	0.024	0.593	0.470	0.037	0.559	0.0067	7.52	
0.6	0.877	$5 \cdot 10^{-3}$	0.865	0.480	0.030	0.551	0.0061	6.84	
0.7	1.16	$1 \cdot 10^{-3}$	1.16	0.484	0.028	0.547	0.0057	6.54	
0.8	1.48	$4 \cdot 10^{-4}$	1.48	0.486	0.027	0.546	0.0053	6.39	
0.9	1.82	$1 \cdot 10^{-4}$	1.82	0.487	0.027	0.545	0.0051	6.30	
1.0	2.19	$4 \cdot 10^{-5}$	2.19	0.488	0.027	0.544	0.0049	6.24	
1.1	2.57	$1 \cdot 10^{-5}$	2.57	0.488	0.027	0.543	0.0048	6.21	
1.2	2.97	$8 \cdot 10^{-6}$	2.97	0.488	0.027	0.543	0.0046	6.17	
1.3	3.39	$4 \cdot 10^{-6}$	3.39	0.489	0.027	0.543	0.0044	6.15	
1.4	3.82	$2 \cdot 10^{-6}$	3.82	0.489	0.026	0.543	0.0042	6.13	
1.5	4.26	$1 \cdot 10^{-6}$	4.26	0.489	0.026	0.542	0.0040	6.12	
1.6	4.72	$6 \cdot 10^{-7}$	4.72	0.489	0.026	0.542	0.0038	6.11	
1.7	5.19	$3 \cdot 10^{-7}$	5.19	0.490	0.025	0.542	0.0036	6.09	
1.8	5.69	$2 \cdot 10^{-7}$	5.69	0.490	0.024	0.542	0.0033	6.09	
1.9	6.17	$1 \cdot 10^{-7}$	6.17	0.490	0.024	0.542	0.0031	6.08	
2.0	6.68	$7 \cdot 10^{-8}$	6.68	0.490	0.023	0.542	0.0029	6.07	

TABLE XVII: Triple points: (ϕ_{cg}, ϕ_{pg}), (ϕ_{cl}, ϕ_{pl}) (ϕ_{cs}, ϕ_{ps}) are the volume fractions of the three coexisting phases, $\widetilde{P}_{tp}$ is the corresponding reduced pressure. Results for $z = z^{(1)}$.

z	q	$\phi_{tp}^{(r)}$	ϕ_{cg}	ϕ_{pg}	ϕ_{cl}	ϕ_{pl}	ϕ_{cs}	ϕ_{ps}	$\widetilde{P}_{tp}$
	0.4	0.467	$5.7 \cdot 10^{-2}$	0.397	0.458	$3.2 \cdot 10^{-2}$	0.566	$4.1 \cdot 10^{-3}$	8.16
	0.5	0.722	$6.4 \cdot 10^{-3}$	0.708	0.479	$1.7 \cdot 10^{-2}$	0.551	$2.7 \cdot 10^{-3}$	6.78
	0.6	1.08	$5.0 \cdot 10^{-4}$	1.08	0.486	$1.0 \cdot 10^{-2}$	0.545	$1.6 \cdot 10^{-3}$	6.31
	0.7	1.54	$5.0 \cdot 10^{-5}$	1.53	0.489	$6.8 \cdot 10^{-3}$	0.543	$8.8 \cdot 10^{-4}$	6.13
	0.8	2.07	$5.2 \cdot 10^{-6}$	2.07	0.490	$4.7 \cdot 10^{-3}$	0.542	$4.9 \cdot 10^{-4}$	6.07
	0.9	2.66	$5.5 \cdot 10^{-7}$	2.67	0.490	$3.3 \cdot 10^{-3}$	0.541	$2.8 \cdot 10^{-4}$	6.04
	1.0	3.32	$7 \cdot 10^{-8}$	3.32	0.491	$2.3 \cdot 10^{-3}$	0.541	$1.6 \cdot 10^{-4}$	6.03
	1.1	4.02	$9 \cdot 10^{-9}$	4.02	0.491	$1.6 \cdot 10^{-3}$	0.541	$9 \cdot 10^{-5}$	6.02
	1.2	4.77	$1 \cdot 10^{-9}$	4.77	0.491	$1.1 \cdot 10^{-3}$	0.541	$5 \cdot 10^{-5}$	6.02
	1.3	5.55	0	5.55	0.491	$8 \cdot 10^{-4}$	0.541	$3 \cdot 10^{-5}$	6.01
	1.4	6.37	0	6.37	0.491	$6 \cdot 10^{-4}$	0.541	$2 \cdot 10^{-5}$	6.01
	1.5	7.23	0	7.23	0.491	$4 \cdot 10^{-4}$	0.541	$8 \cdot 10^{-6}$	6.01
	1.6	8.12	0	8.12	0.491	$3 \cdot 10^{-4}$	0.541	$5 \cdot 10^{-6}$	6.01
	1.7	9.03	0	9.03	0.491	$2 \cdot 10^{-4}$	0.541	$3 \cdot 10^{-6}$	6.01
	1.8	10.0	0	10.0	0.491	$1 \cdot 10^{-4}$	0.541	$1 \cdot 10^{-6}$	6.01
	1.9	11.0	0	11.0	0.491	$9 \cdot 10^{-5}$	0.541	$8 \cdot 10^{-7}$	6.01
	2.0	12.0	0	12.0	0.491	$6 \cdot 10^{-5}$	0.541	$4 \cdot 10^{-7}$	6.01

TABLE XVIII: Triple points: (ϕ_{cg}, ϕ_{pg}), (ϕ_{cl}, ϕ_{pl}) (ϕ_{cs}, ϕ_{ps}) are the volume fractions of the three coexisting phases, $\widetilde{P}_{tp}$ is the corresponding reduced pressure. Results for $z = 0$.

z	q	$\phi_{tp}^{(r)}$	ϕ_{cg}	ϕ_{pg}	ϕ_{cl}	ϕ_{pl}	ϕ_{cs}	ϕ_{ps}	$\widetilde{P}_{tp}$
	0.5	0.811	$1.8 \cdot 10^{-3}$	0.806	0.484	$7.8 \cdot 10^{-3}$	0.547	$9.6 \cdot 10^{-4}$	6.48
	0.6	1.32	$6.6 \cdot 10^{-5}$	1.32	0.489	$2.4 \cdot 10^{-3}$	0.542	$2.0 \cdot 10^{-4}$	6.12
	0.7	2.07	$9.9 \cdot 10^{-7}$	2.07	0.491	$5.8 \cdot 10^{-4}$	0.541	$2.6 \cdot 10^{-5}$	6.03
	0.8	3.08	$9 \cdot 10^{-9}$	3.08	0.491	$1.1 \cdot 10^{-4}$	0.541	$1.9 \cdot 10^{-6}$	6.01
	0.9	4.38	$6 \cdot 10^{-11}$	4.38	0.491	$1.4 \cdot 10^{-5}$	0.541	$9 \cdot 10^{-8}$	6.01
	1.0	6.01	0	6.01	0.491	$1.4 \cdot 10^{-6}$	0.541	$3 \cdot 10^{-9}$	6.01
	1.1	8.00	0	8.00	0.491	$1.0 \cdot 10^{-7}$	0.541	$5 \cdot 10^{-11}$	6.01
	1.2	10.4	0	10.4	0.491	$5 \cdot 10^{-9}$	0.541	$5 \cdot 10^{-13}$	6.01
	1.3	13.2	0	13.2	0.491	$2 \cdot 10^{-10}$	0.541	0	6.01
	1.4	16.5	0	16.5	0.491	$5 \cdot 10^{-12}$	0.541	0	6.01
	1.5	20.3	0	20.3	0.491	$1 \cdot 10^{-13}$	0.541	0	6.01
	1.6	24.6	0	24.6	0.491	0	0.541	0	6.01
	1.7	29.5	0	29.5	0.491	0	0.541	0	6.01
	1.8	35.1	0	35.1	0.491	0	0.541	0	6.01
	1.9	41.2	0	41.2	0.491	0	0.541	0	6.01
	2.0	48.1	0	48.1	0.491	0	0.541	0	6.01

References for the supplementary material

---

* Electronic address: giuseppe.dadamo@sissa.it
† Electronic address: andrea.pelissetto@roma1.infn.it
‡ Electronic address: carlo.pierleoni@aquila.infn.it

[1] G. C. Berry, J. Chem. Phys. **44**, 4550 (1966).
[2] T. Norisuye, K. Kawahara, A. Teramoto, and H. Fujita, J. Chem. Phys **49**, 4330 (1968).
[3] T. Matsumoto, N. Nishioka, and H. Fujita, J. Polym. Sci.: Part A-2 Polym. Phys. **10**,23 (1972).
[4] S. Caracciolo, B. M. Mognetti, and A. Pelissetto, J. Chem. Phys. **128**, 065104 (2008).
[5] G. D'Adamo, A. Pelissetto, and C. Pierleoni, Mol. Phys. **111**, 3372 (2013).
[6] B. Duplantier, J. Phys. (France) **43**, 991 (1982); **47**, 745 (1986); Europhys. Lett. **1**, 491 (1986); J. Chem. Phys. **86**, 4233 (1987); B. Duplantier and G. Jannink, Phys. Rev. Lett. **70**, 3174 (1993).
[7] J. des Cloizeaux and G. Jannink, *Polymers in Solution: Their Modelling and Structure* (Clarendon, Oxford, 1990).
[8] L. Schäfer, *Excluded Volume Effects in Polymer Solutions* (Springer Verlag, Berlin, 1999).
[9] A. D. Sokal, Europhys. Lett. **26**, 661 (1994).
[10] F. J. Wegner, in *Phase Transitions and Critical Phenomena*, edited by C. Domb and M. S. Green (Academic Press, New York, 1976), Vol. 6.
[11] M. Doi and S. F. Edwards, *The Theory of Polymer Dynamics* (Oxford Science, Oxford, 1988).
[12] B. H. Zimm, W. H. Stockmayer, and M. Fixman, J. Chem. Phys. **21**, 1716 (1953).
[13] M. Rubinstein and R. H. Colby, *Polymer Physics* (Oxford Univ. Press, Oxford, 2003).
[14] A. Pelissetto, Macromolecules **39**, 4184 (2006).
[15] S. Caracciolo, B. M. Mognetti, and A. Pelissetto, J. Chem. Phys. **125**, 094903 (2006).
[16] B. Duplantier, G. Jannink, and J. des Cloizeaux, Phys. Rev. Lett. **56**, 2080 (1986).
[17] Y. Nakamura, T. Norisuye, and A. Teramoto, Macromolecules **24**, 4904 (1991).
[18] K. Akasaka, Y. Nakamura, T. Norisuye, and A. Teramoto, Polym. J. **26**, 363 (1994).
[19] A. Pelissetto and J.-P. Hansen, J. Chem. Phys. **122**, 134904 (2005).
[20] P. J. Flory and S. Fisk, J. Chem. Phys. **44**, 2243 (1966).
[21] G. J. Fleer, A. M. Skvortsov, and R. Tuinier, Macromol. Theory Simul. **16**, 531 (2007).
[22] H. N. W. Lekkerkerker and R. Tuinier, *Colloids and the Depletion Interaction*, Lect. Notes Phys. **833** (Springer, Berlin, 2011).
[23] A. Pelissetto, J. Chem. Phys. **129**, 044901 (2008).
[24] G. D'Adamo, A. Pelissetto, and C. Pierleoni, J. Chem. Phys. **139**, 034901 (2013).